UNIVERSITAT POLITÈCNICA DE CATALUNYA BARCELONATECH

A contribution to unobtrusive measurement methods for sleep monitoring based on magnetic induction technique

Hadiseh Mahdavi

Departament d'Enginyeria Electrònica
UNIVERSITAT POLITÈCNICA DE CATALUNYA

A Contribution to Unobtrusive Measurement Methods for Sleep Monitoring Based on Magnetic Induction Technique

Dissertation is submitted for the degree of Doctor of Philosophy

Hadiseh Mahdavi

Director: Prof. Javier Rosell-Ferrer

May 2017

To my parents ...

Declaration

I hereby declare that except where specific reference is made to the work of others, the contents of this dissertation are original and have not been submitted in whole or in part for consideration for any other degree or qualification in this, or any other university. This dissertation is my own work and contains nothing which is the outcome of work done in collaboration with others, except as specified in the text and Acknowledgments.

Hadiseh Mahdavi
May 2017

Acknowledgements

First and foremost I would like to express my sincere gratitude to my advisor Prof. Javier Rosell-Ferrer, for his continuous support, encouragement, inspiration and immense knowledge during my PhD journey. I still have the first Emails we exchanged and remember the first time we met in lovely Barcelona. I will never forget the first time we visited the lab together and his reassuring kind words on that day. He provided me, not only with the PhD opportunity but more importantly, he helped me on making my dreams come true. I left my country with a very little knowledge and experience and he was there for me in every steps of my life as a foreign student, far from my family and friends, in both pleasant and hard moments. He has always been supportive and has given me the freedom to pursue various projects even outside the university, without objection. He is always full of insightful discussions and innovative ideas. Thank you for trusting me.

This thesis has been done in the group of Biomedical and Electronic Instrumentation of the Electronic Engineering Department of Polytechnic University of Barcelona. My deepest gratitude goes to my colleagues, my labmates, my friends... I learned a lot from you all, I shared numerous good moments with you, thanks for the conversations, for the afternoon coffee session, for not spamming the series, for your support... Thank you Tomas for helping me learning Spanish, your indefinite kindness, thanks to Ricardo and Giuseppe and Silvia for their incredible support and friendship... It's impossible to name all; Noelia, Jose, Raul, Fede, Angel, Mark, Albert, Victor, Antonio,... My special thanks go to Alfonso Méndez, thank you for your patience, support and knowledge.

I would also like to express my gratitude to the other professors in the group; Ramon, Lexa, Miguel Angel, Mireia, Juan, Ferran, and Pere.
Particular thanks go to Heiner, my boss at Syntesa, and Andrew my colleague, for their full support and kind patience.
Last but not least, I wish to thank my parents, who taught me to strive more for my dreams... Thanks for always being for me in my ups and downs and for your unconditional support and encouragement. I owe you everything I have.
Thanks to my family, my brothers Ali and Mohammad and my sister Mahdis, for all their support, care and love. And finally my deepest thanks to the love of my life; **VahidReza**... Thanks for your indefinite love and support, helping me in overcoming the difficult moments I had, you shed a light on the darkest nights and brought joy and happiness to my life.
The thesis was partially funded by European 7th framework; Help4Mood.

Abstract

Sleep monitoring is of major importance for various medical areas such as the detection and treatment of sleep disorders, assessment of different medical conditions or medications' effects over sleep quality, and mortality risk assessment associated with sleep patterns in adults and children.
It is a challenging area of medical problems due to both privacy issues and technical considerations. It calls for monitoring methods in which the patient's natural state is less interfered. An ideal device would be non-invasive, minimally restrictive, robust enough to compensate movements of the patients, and would operate without relying on patient's cooperation.
Non-contact methods for monitoring vital signs and physiological activities have been given lots of attention recently. In addition to the sleep monitoring, various other medical applications demand for less-obtrusive continuous respiratory and cardiac activity monitoring methods.
Applications such as home health care, neonates and burned victims monitoring and applications in which using the traditional skin electrodes may worsen or disturb the conditions of the patient, call for new contact-less approaches for monitoring purposes.
This thesis focuses on the design and development of an unobtrusive, vital sign monitoring system particularly suited for long-term monitoring. The system is a low-cost, non-contact planar system designed to be placed under the bed or mattress for applications such as sleep monitoring, neonates monitoring, etc.
The system is based on the magnetic induction sensing method, designed to infer presence on the bed, breathing and cardiac activity and consists of two coils

for excitation and detection. The receiver is an Asymmetric Planar Gradiometer (APG) which has been optimized to minimize the impact of the primary magnetic field. This term (APG) has been interchangeably used with Concentric Planar Gradiometer (CPG) in the text as both reflect our new specific design for the receiver system. The new gradiometer designed using COMSOL to calculate and determine the optimum diameters of the coils to fully cancel the primary field and later implemented on PCB.

The simulations and the experiments showed that the APG has its maximum sensitivity in front of the sensors and moving from the center of the coils causes a decrease in the sensitivity. The designed gradiometer, has no zero sensitivity plane but requires filters to avoid far field interference.

The signal acquisition system has been designed using simple electronics to avoid ending up with a complex expensive system. It consist of a two stage low-noise amplifier (AD8432). The amplified signal is then filtered and introduced to a gain and phase detector (AD8302).

In addition to the developed system, other sensors (BIOPAC MP36's photoplethysmogram, respiratory pressure transducer) have been used as a reference and for comparison reasons.

The practical maximum cancellation ratio obtained in the experiments (through adjusting the coils' position) was measured as 150 times.

Electrical Safety studies indicate that the developed system is safe to be used for continuous monitoring of breathing and cardiac activity for patients, in terms of being exposed to the magnetic fields.

Experiments were conducted using saline solutions and with volunteers on the bed for system characterizations and vital sign detection. The results show that the system placed at 5 cm of the patient's chest, can detect the presence of the patient on the bed, breathing and also cardiac activity. The signal levels decrease with the increment of the distance from the chest.

According to the results, the phase signal received from the magnetic sensor is more sensitive and less noisy than the magnetic modulus signal and both are more sensitive to the vital signs than the pressure sensor. Moreover, comparing the signals of supine and prone position indicates that the signal from prone position contains more information in regards to cardiac activity due to its position advantage. In prone position, the sensors are closer to the heart, to the blood

volume changes in heart's major vessels (Aorta) and to the lung perfusion while in the supine position, the distance is bigger and other structures like vertebral column are located in between.
Breathing causes a movement in patient's back which modifies its distance from sensors. That is why the measured breathing signal could be a combined signal from magnetic coupling and electric field coupling.
Regarding the cardiac signal, the experiments' results show that in some cases/positions the cardiac signal is better detected in either of magnetic phase or modulus signals. The source for the received cardiac signal could be a combination of the changes in the thorax or/and abdomen- which may cause changes in the electric field coupling or surface eddy currents- and in the internal eddy currents produced by conductivity changes originated from lung perfusion, muscle perfusion or blood volume changes in the heart and major vessels.
The designed system has spatial coverage of 8-10 cm for displacement along $\pm X$ assuming that the surface of the bed is on XY plane, Y along the body and X the transverse plane.

Table of contents

List of figures

List of tables

Chapter 1

Introduction

1.1 The need for unobtrusive sleep monitoring

Sleep consumes 1/3 of our lives. It is essential for a person's health and well-being. Yet millions of people do not get enough sleep and many suffer from lack of sleep. For instance, surveys conducted by the NSF[1] (1999-2004) reveal that at least 40 million Americans suffer from over 70 different sleep disorders and 60% of adults report having sleep problems a few nights a week or more. Most of those go undiagnosed and untreated.
In addition, more than 40% of adults experience daytime sleepiness severe enough to interfere with their daily activities at least a few days each month -with 20% reporting problem sleepiness a few days a week or more [1].
Furthermore, 69% of children experience one or more sleep problems a few nights or more during a week. According to the researches done by National heart lung and blood institute[2] the cumulative effects of sleep loss and sleep disorders represent an under-recognized public health problem and have been associated with a wide range of health consequences including an increased risk of hypertension, diabetes, obesity, depression, heart attack, and stroke.

[1] National Sleep Foundation
[2] http://www.nhlbi.nih.gov/index.htm

Almost 20% of all serious car crash injuries in the general population are associated with driver sleepiness [1]. Hundreds of billions of dollars a year are spent on direct medical costs related to sleep disorders such as doctor visits, hospital services, prescriptions, and over-the-counter medications. The effects of sleep loss on work performance may cost 18 billion in lost productivity only in USA [2].
Frequent sleep problems which are reported by 65 percent of Americans including difficulty falling asleep, waking during the night, and waking feeling unrefreshed at least a few times each week, with nearly half (44%) of those saying they experience that sleep problem almost every night [3] .
Sleep-disordered breathing, including obstructive sleep apnea, affects more than 15 percent of the population, and causes daytime sleepiness and associated injuries (e.g., falling asleep while driving), hypertension, cognitive impairment, and is associated with metabolic syndrome, and an increased risk of heart attack, stroke and mortality [1]. In children, sleep-disordered breathing is associated with cardiovascular and metabolic risk factors, attention-related behavioral problems, and poor academic performance. Restless legs syndrome affects over one out of twenty adults, and causes difficulty sleeping and subsequent daytime sleepiness.
Chronic insomnia affects nearly one out of five adults, and is a risk factor for depression, substance abuse, and impaired waking function; co-morbid physical (e.g., cardiopulmonary, chronic pain) and mental (e.g., depression) illnesses may be exacerbated by insomnia.
On the other hand, Major depression affecting between 5 and 10 percent of the population of the European Union during their lifetime [4]. People with depression commonly experience disturbed sleep patterns and the way depression affects sleep varies widely. In addition to clinically defined disorders, chronic sleep deficiency and circadian disruption is an emerging characteristic of modern urban lifestyles and is associated with increase disease risk through multiple complex pathways in all age groups.
Developing a mechanistic understanding of the threat posed by sleep deficiency and circadian disturbance to health, healthy equity, and health disparities is a challenge for biomedical research in many domains. Therefore, the contribution of sleep monitoring, for diagnosing sleep problems to live free of preventable disease, disability, injury, and premature death has been given lots of attentions.

Since a great portion of the population with sleep problems needs continuous monitoring, the techniques for monitoring have to be as unobtrusive as possible. This is to make patients feel relax while testing, lessen the necessity to have complicated clinical environments and minimize the costs. Due to the mentioned reasons, growing interest has emerged for unobtrusive techniques enabling monitoring people during sleep.
The fundamental focus of this thesis is the development of an appropriate technology for the long-term monitoring of sleep and in particular of the vital sign while sleeping. Such a technology is a subject of interest for other medical issues as well.
In home health care application, elderly monitoring, monitoring patients with conditions that can be perturbed or worsened by contact sensors including neonates, infants at risk of sudden infant health syndrome and burn victims, a non-contact heart and respiration status monitoring technology could provide the necessary data with minimum disturbance and complexity for medical experts and ease the decision making process.

1.2 Thesis Objectives

Sleep monitoring is of major importance for various reasons such as the detection and treatment of sleep disorders, assessment of different medical conditions or medications' effects over sleep quality, and mortality risk assessment associated with sleep patterns in adults and children. It is a challenging area of medical problems due to both privacy issues and technical considerations. It calls for monitoring methods in which the patient's natural state is less interfered. An ideal device would be non-invasive, minimally restrictive, robust enough to compensate movements of the patients, and would operate without relying on patient's cooperation.
Motivated by the exposed ideas and mentioned necessities, the main purpose of this PhD thesis is to develop a non-obtrusive and non-contact system based on Magnetic Induction techniques (MI) for detecting vital signals of a patient over the bed. The data detected by the system would be subject to further analysis for sleep assessments while it could also be used in other medical applications. We seek to extend the existing models and compare them our new design to

clarify that what has to be expected from measurements made with MI-based systems and establish the feasibility of measurement with the newly developed instrumentation.
The hypothesis is that a Magnetic Induction System (MIS) will be more sensitive to vital signals and provides more information than the mechanical based systems. This hypothesis is based on the fact that the distribution of eddy currents is in the whole conductive body under test and is not only due to the displacements of the body surface.

In order to accomplish the objectives different steps are outlined:

1. Design and implementation of a monitoring system based on magnetic induction technique for unobtrusive and contact-less vital signs including breathing and cardiac activity
2. Extracting the information related to the respiration and cardiac activity via signal processing
3. Assessment and study the obtained information in order to explore the nature of the received signals; whether the source of such signals is only due to surface body shape changes or conductivity changes contributions or a mix of both
4. Comparison of the results from the developed system with other techniques

The required tasks are summarized below:

- Create three-dimensional models for studying the distribution of electromagnetic fields and eddy currents in a human trunk and perform various simulations of the problem.
- Design and development of a measurement system that allows the evaluation and verification of the simulation results.
- Determining and quantifying the limitations of simulation and experimental measurements.
- Development of experimental and measurement protocols and implementation of them considering the changing parameters of the body postures while sleeping; test and validation.

- Development of comparison experiments in order to relate the available displacement-based methods with our magnetic induction based sensor.

- Signal processing and data assessment

1.3 Thesis outline

The present PhD thesis has been developed in the Electronic and Biomedical Instrumentation group, from the Department of Electronic Engineering at the Universitat Politècnica de Catalunya, Barcelona. This group has been working for more than 30 years in the field of biomedical engineering with special interest in the development of methods and instruments for biomedical applications of electrical impedance tomography and spectroscopy.
This study was partly funded by the European FP7 research program: "**Help4Mood**".
The aim of this project was to develop a system that will help people with major depression recover in their own home. One of the main components of Help4Mood was to develop a personal monitoring system that keeps track of important aspects of behavior such as sleep or activity levels.
The thesis is structured as follows; Chapter 2 presents a brief review of the available systems (commercially or research-only) and existing approaches for non-contact vital sign monitoring. It also includes the theoretical background of magnetic induction technique and the advantages and challenges it offers. Chapter 3 is all about the mathematical models based on finite element method developed for numerical analysis and electromagnetic simulations. The different approaches and tools used as simulation techniques and for model development are explained in detail in this chapter.
In chapter 4, design and implementation of the MI system -from an initial version to an improved prototype- is explained. This section consists of the detailed system description, antenna design and improvements, acquisition system design together with analytical in-depth study of the unwanted coupling mechanisms presents in the system. Subsequently, chapter 5 outlines the results obtained from the experiments performed both by phantoms (saline solution) and volunteers on the bed and also the comparative study between MIS and the pressure-based sensor. Sensitivity of the system to different parameters is explained in this chapter.

Finally, in chapter 6 the general conclusions of the thesis and ideas for future works are presented.

References

[1] HR Colten and MB Altevogt. *Sleep disorders and sleep deprivation: an unmet public health problem.* National Academies Press, Washington, DC, 2006.

[2] Leslie M Swanson, J Todd Arnedt, Mark R Rosekind, Gregory Belenky, Thomas J Balkin, and Christopher Drake. Sleep disorders and work performance: findings from the 2008 National Sleep Foundation Sleep in America poll. *Journal of Sleep Research*, 20(3):487–494, 2011. doi: 10.1111/j.1365-2869.2010.00890.x.

[3] National Sleep Foundation. Sleep In America Poll. Technical Report 202, National Sleep Foundation, 2008.

[4] HJ Moller and V Henkel. *What are the most effective diagnostic and therapeutic strategies for the management of depression in specialist care ?* WHO Regional Office for European Health Evidence Network, Copenhagen, 2005.

Chapter 2

Background

2.1 Review of electromagnetics

Maxwell's equations are a set of four partial differential equations, essential in the study of electromagnetic phenomena: they govern the spatial and temporal evolution of the electrical and magnetic fields. These equations (that published for the first time in differential form in *A Treatise on Electricity and Magnetism*, published by James Clerk Maxwell in 1873) are a synthesis of Gauss's law and Ampère's law and, in fact, unify the concept of electrical field and magnetic field into the wider concept of electromagnetic field.
Maxwell's equations can be formulated in differential or integral form. The differential form is presented here, since it leads to differential equations that the Finite Element Method can handle. For general time-varying fields, Maxwell's

equations can be written as:

$$\nabla \times \mathbf{H} = \mathbf{J} + \frac{\delta \mathbf{D}}{\delta t} \tag{2.1}$$

$$\nabla \times \mathbf{E} = -\frac{\delta \mathbf{B}}{\delta t} \tag{2.2}$$

$$\nabla \cdot \mathbf{D} = \rho \tag{2.3}$$

$$\nabla \cdot \mathbf{B} = 0 \tag{2.4}$$

where:
$\mathbf{H}$ = magnetic field intensity;
$\mathbf{J}$ = current density;
$\mathbf{D}$ = electric flux density;
$\mathbf{E}$ = electric field intensity;
$\mathbf{B}$ = magnetic flux density;
ρ = electric charge density.

The first two equations are also referred to as Maxwell-Ampère's law and Faraday's law, respectively. Equation 2.3 and 2.4 are two forms of Gauss' law: the electric and magnetic form, respectively. Another fundamental equation is the equation of continuity

$$\nabla \cdot \mathbf{J} = -\frac{\delta \rho}{\delta t} \tag{2.5}$$

Out of the five equations mentioned, only three are independent. The first two combined with either the electric form of Gauss' law or the equation of continuity form such an independent system. To obtain a closed system, the equations include constitutive relations that describe the macroscopic properties of the medium. They are given as follow:

$$\begin{aligned} D &= \varepsilon_0 E + P \\ B &= \mu_0 (H + M) \\ J &= \sigma E \end{aligned} \tag{2.6}$$

Where μ_0 is the permeability of vacuum, ε_0 is the permittivity of vacuum and σ is the electrical conductivity. In the SI system, the permeability of vacuum is

$4\pi \times 10^{-7}$ H/m and the ε_0 is 8.85×10^{-12} F/m.
The magnetization vector **M** describes how the material is magnetized when a magnetic field H is present. It can be interpreted as the volume density of magnetic dipole moments. **M** is generally a function of **H**. Permanent magnets, for instance, have a nonzero M also when there is no magnetic field present. In linear materials, the magnetization is directly proportional to the magnetic field, $\mathbf{M} = \chi_{\mathrm{m}} \mathbf{H}$, where χ_{m} is the magnetic susceptibility. For such materials, the constitutive relations are

$$\vec{B} = \mu_0(1 + \chi_{\mathrm{m}})\vec{H} = \mu_r \vec{H} \tag{2.7}$$

The parameter μ_r is the relative permeability of the material. Usually it's a scalar property but can, in the general case, be a 3-by-3 tensor when the material is anisotropic. A consequence of Maxwell's equations is that changes in time of currents and charges are not synchronized with changes of the electromagnetic fields. The changes of the fields are always delayed relative to the changes of the sources, reflecting the finite speed of propagation of electromagnetic waves.
Under the assumption of ignoring this effect, it is possible to obtain the electromagnetic fields by considering stationary currents at every instant. This is called the quasi-static approximation. The approximation is valid provided that the variations in time are small and that the studied geometries are considerably smaller than the wavelength [46]. All simulations were performed considering this approximation.

2.2 Review of sleep measurement technologies

This section provides a brief but comprehensive review of the traditional and modern (clinical and non-clinical) technologies used in sleep monitoring.
As stated before, unobtrusive[1] non-contact vital signal sensing could be a powerful tool in applications where it is not desirable to disturb a subject's physiological and/or emotional state during detection or in other situations where access to the subject is limited.
Many sleep sensing approaches have been proposed for assessment of body be-

[1] Please note that the terms "unobtrusive" and "non-obtrusive" have been used interchangeably in the text as both have been used in literature.

haviors in bed but currently, there is no convenient, non-obtrusive way to assess the quality of sleep. For instance, the assessment of sleep-related disturbances is traditionally performed by Polysomnography. While this method provides a rich data set like breathing, heart rate, blood pressure, etc., it can be done only in the clinic environment with the use of wired sensors and skin electrodes.
Another approach is by wearing and actigraphy devices which is a relatively non-obstructive method. The device monitors activities and later labels periods of low activity as sleep. There are many commercial products like Phillips ActiWatch that has been designed based on actigraphy. Zeo personal coach is another commercial product for sleep monitoring in home environments. It is a headband that users need to wear each night so that it can detect sleep patterns through the electrical signals naturally produced by the brain (EEG).
In the category of wearable sensors or sensors which have a kind of contact with the skin, smart fabrics and interactive textiles have been given lots of attention [1] [2] [3] [4] [5].
Textile based sensors offer a less invasive method of continually monitoring physiological parameters during daily activities [6]. The problem of such kinds of embedded textiles or actigraphy commercial products is that they are rather expensive and still the user needs to wear the device. By focusing on systems which do not require any device to be worn, depending on the detection targets we could consider three types of systems (based on functionality):

- Presence or Bed Occupancy
- Movement detection and classification of sleep periods
- Vital signs monitoring: respiration and/or heart rate

Such a system could be classified in accordance with the following measurement methods:

- Optical
- Radar
- Pressure
- Temperature

- RFID
- Magnetic Induction
- Electrical Impedance Distribution

2.2.1 Optical Approach

One approach to assessing body movement during sleep at night unobtrusively is by using an infrared motion detector (and a ZigBee communication module in case of [7]). The advantage is that it is not necessary to attach any device to the body, but it does not provide any information about breathing or cardiac activity. In a new approach physiological parameters are recorded using an infrared emitting diode and a photo transistor, which are attached between spring coils in the bed mattress [8]. The infrared emitting diode diffuses infrared light into the mattress. The diffusion of this energy is changed by mattress shape variations and spring coil vibrations, which modulate the intensity of the received infrared signal. The intensity is also modulated by physiological parameters such as heart pulse, respiration and body movement. In [9] a contact-less and continuous monitoring of heart rate was done using textile electrodes for the ECG and also with a LED and a photo-diode pair (Photoplethysmography) under the sheet over the mattress. In this method, there is a high dependency between the detected signals and the mattress shape and size which increases the false detections.

2.2.2 Radar Approach

Another interesting method which has been given more attention is using microwave Doppler radar as a remote monitoring technique [10] [11] [12]. A person's chest has a quasi-periodic movement with no net velocity, and according to Doppler theory, reflects the transmitted signal with its phase modulated by the time-varying chest position. As a result, it can be used in respiration and heart rate monitoring [13][14][15]. In this case a company-BiancMed[2]-uses this technology to produce a system for contact-free sleep and breathing monitoring and a number of patent applications have been submitted and published using this technique. Since this method is based on chest movements and surface motions,

[2]http://biancamed.com/

it strongly depends on the patients' movements, body orientation and position regarding the antenna. Patients movements could decrease the accuracy of measurements and the results may very well affect by the motion artifacts.

2.2.3 Pressure Approach, Ballistocardiography (BCG)

Another method used for sleep monitoring, which is widely used, is to instrument a mattress with different types of pressure sensors and monitor body movements and vital signs. This technique is commercially available and has been widely used, some examples are S4Sensors, Contin bed and chair monitor system, Xsensors, Early Sense, etc. These systems are able to detect -at least- the presence of the patient over the bed and movement and/or cardiac and respiratory related mechanical signals.
In [16] the authors used four vinyl tubes of 2 mm inner diameters Flat-type sensor (Thickness: 8 mm) filled with silicon-oil that sandwiched by two acrylic plates, the width of which is aligned with the bed size. One end of each tube is connected to a pressure sensor and the other end is closed. This flat-type sensor is set under a pillow or a bed mat. The inner pressure in each tube is changed in accordance with respiration, cardiac beating and snore, and thus such information can be detected by using appropriate signal processing. Another novel approach is bed-type sensor system using the air-mattress with balancing tube method for non-invasive monitoring of heartbeat, respiration, and events of snoring, sleep apnea and body movement of the subjects. This system consists of multiple cylindrical air cells. The physiological signals were measured by the changes in pressure difference between the sensor cells [17].
In [18], the authors use pressure and temperature sensors laid out in a grid pattern in the mattress to determine the quality of sleep. Bench testing has shown that heart rate can be measured reliably and is not significantly affected by body orientation. The NAPS (Non-invasive Analysis of Physiological Signals) is a low-cost physiological sensor-suite that can passively acquire important physiological and environmental characteristics [19]. The NAPS suite allows subjects to simply lie on a mattress pad, embedded with vibration sensors, to obtain multidimensional data (e.g., body temperature, heart rate, respiration rate, positional mapping and movement).
Emfit sensors (commercially available) are made of Ferroelectrets. The Emfit

products are based on an elastic, permanently charged ferro-electret film that converts mechanical stress into proportional electrical energy and conversely. Emfit mechanically expands when voltages of opposite polarities are applied. Using this sensor, numerous movement monitors, epilepsy and non-contact vital signal monitoring systems have been designed. In a study of mechanical sensors [20], an electret foil of 30cm x 60cm was simply placed in the thorax region under a thin mattress on top of the existing sheet. In [21], a pressure-sensor array was used and cross-correlation techniques were applied to realign polarity-adjusted signals to create a map of delays across the torso. The map of delays between the pressure sensors' signals reveals important information about movement timing in the torso while breathing.
In [22], FlexiForce Sensor has been used along with a driving circuit and a Silab's C8051F020 Micro controller development board. The bed sensor was integrated with a wireless system for a smart digital home monitoring.
Another method is employing load cells installed at the corners of the bed, allowing both detection of movements and classification of movement types. The system focuses on identifying when a movement occurs based on the forces sensed by the load cells. The movement detection approach estimates the energy in each load cell signal over short segments to capture the variations caused by movement [23].
Applying pressure sensors has been a relatively successful method among others considering that each configuration has its own limitation and problems. The commercial systems are very expensive, some others need complicated installation process which can not be done easily and without expertise. Moreover, few of these approaches present an accurate satisfying signal of cardiac activity or respiration.

2.2.4 Temperature Approach

Temperature regulation in a body can also be used to monitor sleep quality and vital sign detection. The mean thermal signal of the nostril region carries the breathing information. Skin temperature increases during sleep onset and decreases during wake-up. These indicators could be used for monitoring aims. However, it should be noted that the temperature variations can mainly be measured under controlled laboratory conditions [24].

2.2.5 RFID

RFID could also be used to assess movements in the bed. Active RFID tags may be used which combine passive UHF RFID technology with sensors to balance energy independence with sensing potential [25]. In this method, different algorithms for classifying various sleep postures should be used. Commonly in these systems, false detections in comparison with gold standards or with pressure sensors detected signals are higher and the system do not provide any information of breathing or cardiac activity.

2.2.6 Magnetic Induction

This Technique mainly focuses on vital sign monitoring rather than movement or presence detection. It is known that breathing and heart activity change the electrical impedance distribution in the human body over the time due to ventilation (the air in the lungs decreases the lung impedance) and blood shifts (blood perfusion decreases the organ's impedance) [26]. Thus, it is possible to detect both important vital parameters by measuring the impedance of the thorax or the region around the lungs and the heart.
Magnetic Induction methods are based on inducing currents into the human body with one or more coils. The conductivity of tissues inside the body alters the induced eddy current. The re-induced magnetic fields generated through these currents could be measured with properly designed receiving system. A single coil could be used for both signal transmission and detection. The coils can be embedded into the mattress. The flexible coils are able to tolerate bending due to the subjects' weight and movement, and provide a continuous monitoring of the patient breathing pattern or cardiac activity [27] [28] [29] [30] [31].
More sophisticated system using multi-frequency (spectroscopy) techniques have been developed in [32] [33] [34]. An alternative is to measure the changes in frequency or losses in an oscillator. [35] uses an LC oscillator to measure the impedance change of chest and wrist due to the heart or lung activity with capacitive and inductive electrodes.
The principle of this technique has been used extensively for the nondestructive testing of metals. As stated before the idea of using a similar method for medical applications is very attractive. This technique provides complete contact-free

measurement setup, the coil(s) can be easily integrated into beds, mattresses or chairs and it provides a continuous monitoring method without disturbing the patient's state by cables or attached electronics.

2.3 Magnetic Induction (MI) Method

When a conductive object is placed in a time varying magnetic field, eddy currents are induced in the body which perturbs that primary magnetic field. These currents, which are in accordance with the laws of Faraday and Lenz, produce a magnetic field that can be detected by a properly designed receiver system (see figure 2.1).

This fact has been verified theoretically and experimentally and has been used extensively for non-destructive testing of metals and the idea of applying a similar method in the biomedical field was very attractive especially in medical imaging. The advantage of magnetic induction systems over other methods (electrical impedance tomography for instance) is that no direct contact is required with the object and the magnetic fields are not blocked by poorly conducting tissues such as bones.

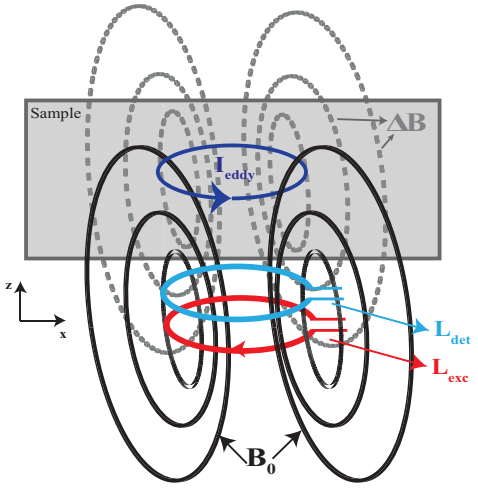

Fig. 2.1 Physical principle of magnetic induction measurement technique

2.3.1 Measurement basis

By injecting a time-varying current in to an excitation antenna (coil), a magnetic flux, also called the primary magnetic field is produced. The magnetic field induces eddy currents in conductive materials. The amplitude of the eddy current is proportional to the magnetic flux density and the conductivity of the material. This induced eddy currents generates itself a further magnetic field call secondary magnetic field which could be measured by a suitable receiver antenna. This measured signal is a function of the conductivity, geometry of the tissue and the geometry of the excitation and detection antennas.
For a cylindrical sample with radius R and thickness t ($t \prec\prec a$) positioned coaxially halfway between two small coils with distance 2a (figure 2.2, the relative change of the magnetic field in the receiver coil and, hence, the corresponding relative voltage change can be expressed by [26][36][37]:

$$\frac{\Delta B_0}{B_0} = \frac{\Delta V_0}{V_0} = \frac{a^3 t}{2}\left\{\chi_m \frac{R^2(8a^2 - R^2)}{(a^2+R^2)^4} - j(\sigma + j\omega\varepsilon_0\varepsilon_r)\omega\mu_0 \times \left[\frac{1}{a^2} - \frac{a^2+2R^2}{(a^2+R^2)^2}\right]\right\} \tag{2.8}$$

where χ_m denotes the magnetic susceptibility of the material. Equation 2.8 is only valid for small perturbation, i.e., if the alteration of the excitation field is negligible and if μ_r is close to 1, which is the case for biological tissues.

Simplifying the equation 2.8 for a sample of material placed between an excitation coil and a sensing coil, and if the skin depth of the electromagnetic field in the material is larger than the dimension of the sample, we have [26]:

$$\Delta B_0/_B \propto \omega(\omega\varepsilon_0\varepsilon_r - j\sigma) \tag{2.9}$$

where σ is the conductivity of the sample, ε_r is its relative permittivity, ε_0 is the permittivity of free space, ω is the angular frequency of the excitation and $j = \sqrt{-1}$. Thus, the conduction currents induced in the sample cause a component of ΔB_0 which is proportional to frequency and lags the primary field, B_0, by 90°. In general, ΔB_0 will have real and imaginary components representing the permittivity and conductivity of the sample respectively [38] (Figure 2.3). For biological tissues, the conductivity (imaginary) component will normally be dominant [38].

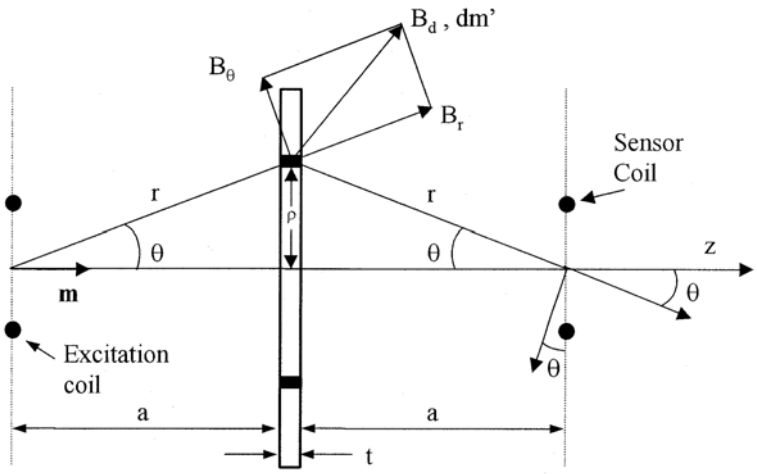

Fig. 2.2 Model of the electromagnetic coupling between a cylindrical sample and a coil system [33]

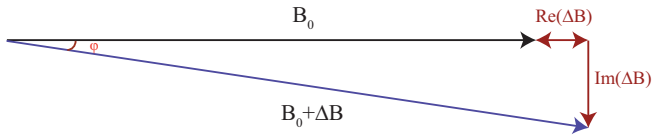

Fig. 2.3 Phasor diagram representing the primary B_0 and secondary (ΔB_0) magnetic fields detected. The total detected field ($\Delta B_0 + B_0$) lags the primary field by an angle φ [38]

2.3.2 Alternative measurement systems

As a general challenge, in biomedical applications, with tissue conductivity in the range (typically $\ll 1 S/m$), the signal ΔB_0 induced by the eddy currents is typically much smaller than the primary background signal B_0, i.e., $|\Delta B_0/B_0|$ is generally $\ll 1$ [38] and increases in proportion to the excitation frequency. Moreover, if the phasor representations are used, the imaginary part of the expression $\mathrm{Im}|\Delta B_0/B_0|$ increases with increasing tissue conductivity σ, i.e., $\mathrm{Im}(\Delta B_0/B_0) \propto \sigma$, whereas the real component $Re(\Delta B_0/B_0)$ is relatively insensitive to changes in tissue conductivity. Thus, for conductivity change monitoring, it is the imaginary part or the phase shift that dominantly contains the desired information. The conductivities of biological tissues are many orders of magnitude lower than metals, this means that the secondary signals to be measured are very weak. The perturbation field (secondary field) could be measured via one or an array of re-

ceiver coils.
In the single coil method, the coil is part of a Colpitts oscillator sending out the alternating magnetic field with a frequency usually between 4 to 10 MHz. The induced secondary field is measured indirectly by the effective impedance change produced by it [30]. However, developed systems by this technique suffer from several artifacts. Moving an object relatively to the coil poses a change in the conductivity distribution of the region measured by the sensor while on the other hand, parasitic stray capacitance acts as a proximity sensor. Using two or more coils (array of coils) has been investigated in various measurement systems designed for vital sign monitoring and tomography. The secondary induced field in this method is directly measured by a (or a set of) receiver coils. Relative voltage changes $\Delta V_0/V_0$ is acquired from the receive(s), ΔV_0 is the voltage change and V_0 is the induced voltage in one receiver coil in the absence of a perturbation.

2.3.3 Primary field cancellation methods

Considering the small secondary signal and the large background signal, the design process, especially the coil's configuration, is very critical in the overall performance of the MI systems. When using, for example, a coaxial pair of coils, $\Delta V_0/V_0$ can be as low as 10^{-7} [37]. Digital processing of such signals requires an impractically high dynamic range of the ADCs. Therefore, it is recommended [39] to reduce the induced voltage V_0 in the unloaded system while preserving maximum sensitivity to conductivity changes.
The three possible cancellation methods are:

1. producing zero magnetic flux in the unperturbed situation by orientation of the receiver coil (zero flux coil, ZFC) [40]

2. subtraction of the signals in a pair of differential coils (gradiometer)

3. electronic subtraction of V_0 by adding $-V_0$ from a controllable signal generator

Since the first and second methods are easier to implement and more importantly they cancel the primary field (voltage) at an earlier stage, they are preferable regarding the third method.

2.3.3.1 Zero flux coil

Zero flux coil is, in fact, the cancellation of the primary field by aligning the receiver coil(s) along the magnetic lines of the primary excitation field such that there is no net flux through the coil (see figure 2.4). In [41] the authors described a system utilizing this principle. Their adoption of an annular array geometry allowed primary field compensation only for the two sensor coils adjacent to the excitation coil. In [40] the principle was extended to allow primary field compensation for an array of the excitation coil and sensor coil where all the coils are placed on a common plane.

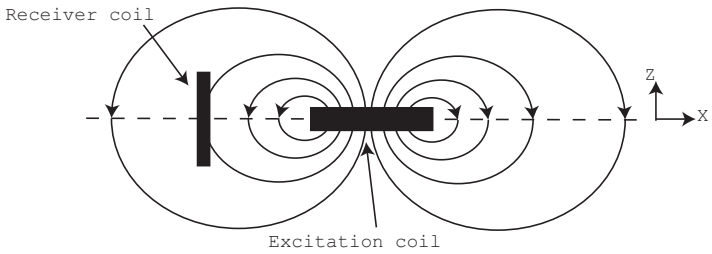

Fig. 2.4 Sensor coil alignment for zero sensitivity to excitation field, adapted from [40]

2.3.3.2 Gradiometer

This approach consists of subtracting from the received signal a voltage as close as possible (in the practical situation) to the V_0 while maintaining the ΔV_0 at the original level to keep the sensitivity. This can be achieved by connecting two coils in counter-phase. Ideally, the voltage induced in the absence of the object should be zero when the gradiometer is adjusted because both coils receive the same magnetic flux if they are placed symmetrically regarding the excitation coil (figure 2.5). Gradiometers could be either coaxial or planar, symmetric or asymmetric (figures 2.6 and 2.7).

2.3.3.3 Comparison of cancellation methods

Comparing the two mentioned methods, in the case of ZFC, no voltage is induced by the primary field. This is an advantage over the gradiometer structure because

the subtraction of two relatively high voltages in gradiometer coils is never perfect leaving a residual voltage, that also could have some drifts. On the other hand, a disadvantage of the ZFC is the higher susceptibility to interferences from far RF sources [39] which in the gradiometer such interferences are canceled up to a rather high degree.
The coaxial type of the gradiometer and the ZFC are not suitable for being placed under the bed or mattress. While the symmetric planar gradiometer, due to its intrinsic 2D structure, seems a suitable option for our application, it shows a zero sensitivity plane in the center which is totally undesirable. **O**ur approach was to design an **A**symmetric **P**lanar **G**radiometer (APG) in order to address the mentioned challenges. Although the asymmetric nature of APG, will make it susceptible to interference from far RF sources. This term (APG) has been interchangeably used with the term Concentric Planar Gradiometer (CPG) in the text as both reflect our new specific design for the receiver system.

2.3.4 Exposure to electromagnetic field

2.3.4.1 Limitations and standards

Magnetic induction monitoring systems are based on the exposure of electromagnetic fields, so the limitations and standards for the exposure to these fields should be considered in the design process. Exposure to time-varying electromagnetic field results in internal body currents and energy absorption in tissues. The quantity of energy absorption and level of internal currents depend on the coupling mechanisms and the frequency involved.
Specific absorption rate (SAR) is a measure of the rate at which energy is absorbed by the body when exposed to a radio frequency (RF) electromagnetic field; It is defined as the power absorbed per mass of tissue and has units of watts per kilogram (W/kg). SAR is usually averaged either over the whole body, or over a small sample volume (typically 1 g or 10 g of tissue). The value cited is then the maximum level measured in the body part studied over the stated volume or mass. The most commonly used safety standards are the ANSI/IEEE C95.1 [43] and ICNIRP [44]. Basic restrictions for frequencies up to 10 GHz prescribed in the ICNIRP standard [44], are given in table 2.1. In accordance with ICNIRP recommendations, the maximum field strength is limited by the specific absorp-

tion ratio (SAR) which shall not exceed 2 W/Kg for head and torso. As a safety requirement, we have studied the estimated SAR of the developed sensor system which will be explained in chapter 3.

Table 2.1 ICNIRP basic restrictions for time-varying electric and magnetic fields for frequencies up to 10 GHz

Exposure	Frequency Range	Current density J for head and trunk mA/m$\hat{2}$	Whole-body average-SAR W/Kg	Localized-SAR for head and trunk W/Kg
Occupational exposure	Up to 1 Hz	40	–	
	1-4 Hz	40/f	–	
	4 Hz-1 kHz	10	–	
	1-100 kHz	f/100	–	
	100 kHz-10 MHz	f/100	0.4	10
	10 MHz-10 GHz	–	0.4	10
General public exposure	Up to 1 Hz	8	–	
	1-4 Hz	8/f	–	
	4Hz-1 kHz	2	–	
	1-100 kHz	f/500	–	
	100 kHz-10 MHz	f/500	0.08	2
	10 MHz-10 GHz	–	0.08	2

The IEEE safety standard, on the other hand, is given in terms of maximum permissible exposures (MPE) of incident external fields for controlled and uncontrolled environments corresponding to occupational and general public exposures (table 2.2).

2.3.5 Mathematical Models (FEM method)

Computer modeling of electromagnetic fields distributed in biological tissues is a very important step to have an estimation of the field lines and their distribution and intensity, the sensitivity of the system to various parameters, induced cur-

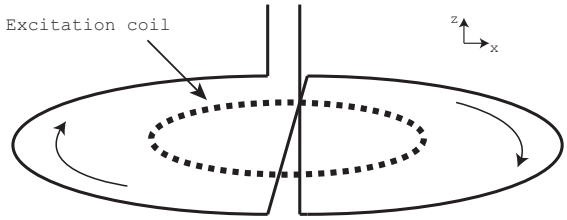

Fig. 2.5 Sample gradiometer coils arranged horizontally, adapted from [42]

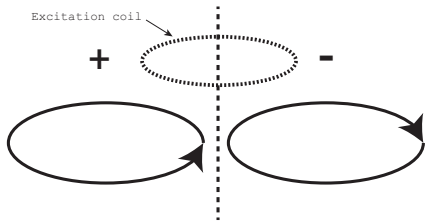

Fig. 2.6 Planar symmetric gradiometer

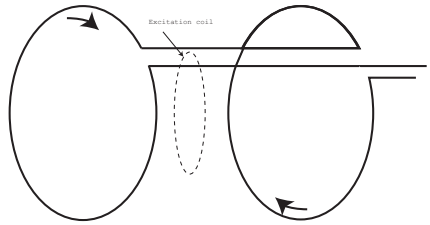

Fig. 2.7 Coaxial symmetric gradiometer

Table 2.2 The IEEE maximum permissible exposure limits for controlled and uncontrolled environments

Controlled environments (Occupational)				**Uncontrolled environments(General Public)**		
Frequency range(MHz)	**E (V/m)**	**H (A/m)**	**Power density (mW/cm^2)**	**E (V/m)**	**H (A/M)**	**Power density (mW/cm^2)**
0.003-0.1	614	163	–	614	163	–
0.1-3.0	614	16.3/f	–	614 (up to 1.34MHz) 823.8/f (from 1.34-3.0 MHz)	16.3/f	–
3-30	1842/f	16.3/f	–	823.8/f (from 1.34-3.0 MHz)	16.3/f	–
30-100	61.4	16.3/f	–	27.5	158.3/f	–
100-300	61.4	0.163	1	27.5	0.0729	0.2
300-3000	–	–	f/300	–	–	f/1500
3000-15000	–	–	10	–	–	f/1500
15000-300000	–	–	10	–	–	10

rents and etc. One of the solutions for solving these kinds of problems is Finite Element Method (FEM) which is a powerful numerical method. The limitations of the human mind are such that it cannot grasp the behavior of its complex surrounding and creations in one operation. Thus the process of subdividing all systems into their individual components or "elements" whose behavior is readily understood, and then rebuilding the original system from such components to study its behavior in a natural way [45]. One definition for FEM could be [45]: a method of approximation to continuum problems such that

1. the continuum is divided in to a finite number of parts (elements), the behavior of which is specified by a finite number of parameters, and

2. the solution of the complete system as an assembly of its elements follows precisely the same rules as those applicable to standard discrete problems.

The key feature of the FEM is the discretization through the creation of a mesh made up of primitives (finite elements) in a coded manner (triangles and quadrangles in 2D domains, hexahedrons, and tetrahedrons in 3D domains). On each element characterized by this elemental shape, the solution of the problem is assumed to be expressed by the linear combination of functions called basis functions or shape functions. From several commercial FEM software packages, we have chosen the "COMSOL Multiphysics" (from now on used as COMSOL) in order to simulate our problem. COMSOL is a powerful interactive finite element analysis, solver and Simulation software package for various physics and engineering applications, especially coupled phenomena, or multiphysics. Although in this software the user has the options and features to go through a complete process of simulation; 2D or 3D design and modeling, adding boundary conditions, parametric simulations and etc., its generally a bit complex to design the 3D model in COMSOL itself. There is an import module which users can import a CAD model to COMSOL and later apply the conditions and simulate the problem within it. At the time of our work with the version available and considering that our desired model is a human trunk with its complexities, besides FEM software we have used other softwares (Solidworks, Simpleware,...) and methods for modeling the body. Other softwares used in this work for different other simulations, are ORCAD, LabView and MATLAB.
It's important to note that like the majority of software packages, before trying

to simulate a problem, the theory and the concepts behind the problem should be carefully understood to avoid false or irrelevant results, so before going to the details of the simulation steps and results, a short review of electromagnetic, theories and formulas - which have been applied in FEM modelling and simulations- is explained in the next section.

References

[1] A Lymberis and R Paradiso. Smart Fabrics and Interactive Textile Enabling Wearable Personal Applications: R&D State of the Art and Future Challenges. In *30th Annual International Conference of the IEEE Engineering in Medicine and Biology Society*, volume 2008, pages 5270–3, jan 2008. ISBN 9781424418152. doi: 10.1109/IEMBS.2008.4650403.

[2] Shirley Coyle, King-Tong Lau, Niall Moyna, Donal O'Gorman, Dermot Diamond, Fabio Di Francesco, Daniele Costanzo, Pietro Salvo, Maria Giovanna Trivella, Danilo Emilio De Rossi, Nicola Taccini, Rita Paradiso, Jacque-André Porchet, Andrea Ridolfi, Jean Luprano, Cyril Chuzel, Thierry Lanier, Frdéric Revol-Cavalier, Sébastien Schoumacker, Véronique Mourier, Isabelle Chartier, Reynald Convert, Henri De-Moncuit, and Christina Bini. BIOTEX-Biosensing Textiles For Personalised Healthcare Management. *IEEE Transactions On Information Technology In Biomedicine*, 14(2):364–70, mar 2010. ISSN 1558-0032. doi: 10.1109/TITB.2009.2038484.

[3] T Klingeberg and M Schilling. Mobile wearable device for long term monitoring of vital signs. *Computer methods and programs in biomedicine*, 106(2):89–96, may 2012. ISSN 1872-7565. doi: 10.1016/j.cmpb.2011.12.009. URL http://www.ncbi.nlm.nih.gov/pubmed/22285459.

[4] Mahsan Rofouei, Mike Sinclair, Ray Bittner, Tom Blank, Nick Saw, Gerald DeJean, and Jeff Heffron. A Non-invasive Wearable Neck-Cuff System for Real-Time Sleep Monitoring. *2011 International Conference on Body Sensor Networks*, pages 156–161, may 2011. doi: 10.1109/BSN.2011.38. URL http://ieeexplore.ieee.org/lpdocs/epic03/wrapper.htm?arnumber=5955315.

[5] T. Suzuki, H. Tanaka, S. Minami, H. Yamada, and T. Miyata. Wearable wireless vital monitoring technology for smart health care. In *2013 7th International Symposium on Medical Information and Communication Technology (ISMICT)*, pages 1–4. Ieee, mar 2013. ISBN 978-1-4673-5772-2. doi: 10.1109/ISMICT.2013.6521687. URL http://ieeexplore.ieee.org/lpdocs/epic03/wrapper.htm?arnumber=6521687.

[6] Marco Di Rienzo, Paolo Meriggi, Francesco Rizzo, Paolo Castiglioni, Carolina Lombardi, Maurizio Ferratini, and Gianfranco Parati. Textile Technology For The Vital Signs Monitoring In Telemedicine And Extreme Environments. *IEEE Transactions On Information Technology In Biomedicine*, 14(3):711–7, may 2010. ISSN 1558-0032. doi: 10.1109/TITB.2010.2048921.

[7] J. M. Choi, B. O. Kim, B. S. Hwang, R. H. Sohn, and K. S. Park. Unobtrusive Body Movement Monitoring during Sleep using Infrared Motion Detector And ZigBee Protocol. *3rd IEEE/EMBS International Symposium On Medical Devices and Biosensors*, pages 32–33, sep 2006. doi: 10.1109/ISSMDBS.2006.360090.

[8] Hiromichi Maki, Hidekuni Ogawa, Sosuke Tsukamoto, Yoshiharu Yonezawa, and W Morton Caldwell. A System For Monitoring Cardiac Vibration, Respiration and Body Movement in Bed Using an Infrared. In *32nd Annual International Conference of the IEEE Engineering in Medicine and Biology Society*, pages 5197–200, jan 2010. doi: 10.1109/IEMBS.2010.5626099.

[9] M Wong, E Pickwell-MacPherson, and Y Zhang. Contactless And Continuous Monitoring Of Heart Rate Based on Photoplethysmography On a Mattress. *Physiological measurement*, 31(7):1065–74, jul 2010. ISSN 1361-6579. doi: 10.1088/0967-3334/31/7/014.

[10] Changzhi Li, Victor M. Lubecke, Olga Boric-Lubecke, and Jenshan Lin. A Review on Recent Advances in Doppler Radar Sensors for Noncontact Healthcare Monitoring. *IEEE Transactions on Microwave Theory and Techniques*, 61(2013):2046–2060, 2013.

[11] R. R. Fletcher and Sarang Kulkarni. Wearable doppler radar with integrated antenna for patient vital sign monitoring. *2010 IEEE Radio and Wireless Symposium, RWW 2010 - Paper Digest*, pages 276–279, 2010. doi: 10.1109/RWS.2010.5434220.

[12] Rich Fletcher and Jing Han. Low-cost differential front-end for doppler radar vital sign monitoring. *IEEE MTT-S International Microwave Symposium Digest*, pages 1325–1328, 2009. ISSN 0149645X. doi: 10.1109/MWSYM.2009.5165949.

[13] Dany Obeid, Sarah Samad, Sawsan Sadek, and Gheorghe Zaharia. Position-Free Vital Sign Monitoring: Measurements and Processing. In Christoph Hintermüller, editor, *Advanced Biosignal Processing and Diagnostic Methods*, chapter 2. InTech, 2016. ISBN 10.5772/63915. URL http://www.intechopen.com/books/advanced-biosignal-processing-and-diagnostic-methods/position-free-vital-sign-monitoring-measurements-and-processing.

[14] G. Obeid, D. and Sadek, S. and Zaharia, G. and El Zein. A Tunable-Frequency System For Touch-Less Heartbeat Detection And HRV Extraction. In *International Symposium on Signals, Circuits and Systems*, jul 2009. ISBN 978-1-4244-3785-6. doi: 10.1109/ISSCS.2009.5206132.

[15] Shuhei Yamada, Mingqi Chen, and Victor Lubecke. Sub-μW Signal Power Doppler Radar Heart Rate Detection. In *Asia-Pacific Microwave Conference*, pages 51–54. IEEE, dec 2006. ISBN 978-4-902339-08-6. doi: 10.1109/APMC.2006.4429377.

[16] Kosuke Motoi, Mitsuhiro Ogawa, Hiroshi Ueno, Yutaka Kuwae, Akira Ikarashi, Tadahiko Yuji, Yuji Higashi, Shinobu Tanaka, Toshiro Fujimoto, Hidetsugu Asanoi, and Ken-ichi Yamakoshi. A fully automated health-care monitoring at home without attachment of any biological sensors and its clinical evaluation. In *31st Annual International Conference of the IEEE Engineering in Medicine and Biology Society*, pages 4323–6, jan 2009. doi: 10.1109/IEMBS.2009.5333712.

[17] Jae Hyuk Shin, Young Joon Chee, Do-Un Jeong, and Kwang Suk Park. Nonconstrained Sleep Monitoring System And Algorithms Using air-Mattress With Balancing Tube Method. *IEEE Transactions on Information Technology In Biomedicine*, 14(1): 147–56, jan 2010. ISSN 1558-0032. doi: 10.1109/TITB.2009.2034011.

[18] H F Machiel Van Der Loos, Hisato Kobayashi, Gregory Liu, and Ying Yu Tai. Unobtrusive Vital Signs Monitoring From a Multi sensor Bed Sheet. In *Rehabilitation Engineering and Assistive Technology Society of North America*, pages 218–220, 2001.

[19] David C Mack, Steve W Kell, Majd Alwan, Beverely Turner, and Robin A Felder. Non-Invasive Analysis of Physiological Signals (NAPS): A Vibration Sensor That Passively Detects Heart and Respiration Rates as Part of a Sensor Suite for Medical Monitoring. In *Bioengineering Conference*, 2003.

[20] Xavier L Aubert and Andreas Brauers. Estimation Of Vital Signs In Bed From A Single Unobtrusive Mechanical Sensor: Algorithms And Real-Life Evaluation. In *Annual International Conference of the IEEE Engineering in Medicine and Biology Society*, volume 2008, pages 4744–7, jan 2008. doi: 10.1109/IEMBS.2008.4650273.

[21] Daphne I Townsend, Megan Holtzman, Rafik Goubran, Monique Frize, Senior Member, and Frank Knoefel. Measurement of Torso Movement With Delay Mapping Using an Unobtrusive Pressure-Sensor Array. *IEEE Transactions On Instrumentation And Measurement*, 60(5):1751–1760, 2010.

[22] A. Gaddam, S. C. Mukhopadhyay, and G. Sen Gupta. Necessity Of A Bed-Sensor In A Smart Digital Home To Care For Elder-People. In *IEEE Sensors Conference*, pages 1340–1343, oct 2008. ISBN 978-1-4244-2580-8. doi: 10.1109/ICSENS.2008.4716693.

[23] Adriana M Adami, Misha Pavel, Tamara L Hayes, and Clifford M Singer. Detection of movement in bed using unobtrusive load cell sensors. *IEEE Tansactions on Information Technology in Biomedicine*, 14(2):481–490, 2010.

[24] Jin Fei and Ioannis Pavlidis. Thermistor at a distance: unobtrusive measurement of breathing. *IEEE Transactions on Biomedical Engineering*, 57(4):988–98, apr 2010. ISSN 1558-2531. doi: 10.1109/TBME.2009.2032415.

[25] Enamul Hoque, Robert F Dickerson, and John A Stankovic. Monitoring Body Positions and Movements During Sleep using WISPs. In *Wireless Health*, 2010.

[26] H Griffiths, W.R. Stewart, and W Gough. Magnetic Induction Tomography: A Measuring System for Biological Tissues. *Annals of the New York Academy of Sciences*, 1999.

[27] A. Richer and A. Adler. Eddy Current Based Flexible Sensor For Contactless Measurement of Breathing. In *IEEE Instrumentation and Measurement Technology Conference*, number May, pages 257–260. IEEE, 2005. ISBN 0-7803-8879-8. doi: 10.1109/IMTC.2005.1604112.

[28] Rosalyn Seeton and Andy Adler. Sensitivity Of a Single Coil Electromagnetic Sensor For Non-Contact Monitoring Of Breathing. In *IEEE Conference of Engineering in Medicine and Biology Society.*, volume 2008, pages 518–21, jan 2008. doi: 10.1109/IEMBS.2008.4649204.

[29] Daniel Teichmann, Andreas Kuhn, Steffen Leonhardt, and Marian Walter. The MAIN Shirt: a textile-integrated magnetic induction sensor array. *Sensors (Basel, Switzerland)*, 14(1):1039–56, jan 2014. ISSN 1424-8220. doi: 10.3390/s140101039. URL http://www.pubmedcentral.nih.gov/articlerender.fcgi?artid=3926601&tool=pmcentrez&rendertype=abstract.

[30] Daniel Teichmann, Jerome Foussier, and Steffen Leonhardt. Respiration monitoring based on magnetic induction using a single coil. In *Biomedical Circuits and Systems Conference (BioCAS)*, number 2, pages 37–40. IEEE, nov 2010. ISBN 978-1-4244-7269-7. doi: 10.1109/BIOCAS.2010.5709565.

[31] Daniel Teichmann, Student Member, Jing Jia, Steffen Leonhardt, and Senior Member. Noncontact Monitoring of Cardiorespiratory Activity by Electromagnetic Coupling. 60(8): 2142–2152, 2013.

[32] J Rosell-Ferrer, R Merwa, P Brunner, and H Scharfetter. A multifrequency magnetic induction tomography system using planar gradiometers: data collection and calibration. *Physiological Measurement*, 27(5):S271–S280, 2006.

[33] Hermann Scharfetter, Roberto Casañas, and Javier Rosell. Biological Tissue Characterization By Magnetic Induction Spectroscopy (MIS): Requirements And Limitations. *IEEE Transactions on Biomedical Engineering*, 50(7):870–80, jul 2003. ISSN 0018-9294. doi: 10.1109/TBME.2003.813533.

[34] Do˘ ga Gürsoy and Hermann Scharfetter. Magnetic Induction Pneumography : A Planar Coil System For Continuous Monitoring Of Lung Function Via Contactless Measurements. *Electrical Bioimpedance*, 1(26283):56 – 62, 2010.

[35] Joon Ho Oum, Hyunji Koo, and Songcheol Hong. Non-contact Heartbeat Sensor using LC oscillator circuit. In *30Annual International Conference of the IEEE Engineering in Medicine and Biology Society*, volume 2008, pages 4455–8, jan 2008. doi: 10.1109/IEMBS.2008.4650200.

[36] Roberto Casañas, Hermann Scharfetter, A Altes, and Javier Rosell. Magnetic induction system for noninvasive measurement of susceptibility and conductivity of biological tissues. In *XI ICEBI*, pages 623–626, 2001.

[37] Hermann Scharfetter, Roberto Casañas, and Javier Rosell. Biological tissue characterization by magnetic induction spectroscopy (MIS): requirements and limitations. *IEEE Transactions on Biomedical Engineering*, 50(7):870–880, 2003.

[38] H Griffiths. Magnetic induction tomography. *Measurement Science and Technology*, 12 (8):1126–1131, 2001. ISSN 09673334.

[39] Hermann Scharfetter, Robert Merwa, and Karl Pilz. A new type of gradiometer for the receiving circuit of magnetic induction tomography (MIT). *Physiological measurement*, 26(2):S307–18, 2005. ISSN 0967-3334. doi: 10.1088/0967-3334/26/2/028. URL http://www.ncbi.nlm.nih.gov/pubmed/15798243.

[40] S Watson, A Morris, R J Williams, H Griffiths, and W Gough. A primary field compensation scheme for planar array magnetic induction tomography. *Physiological Measurement*, 25(1):271–279, 2004. ISSN 0967-3334. doi: 10.1088/0967-3334/25/1/031. URL http://stacks.iop.org/0967-3334/25/i=1/a=031?key=crossref.81cc097828e77ec388b778bb20686a2b.

[41] Z Z Yu and A J Peyton. Development of sensor arrays for electromagnetic inductive tomography: compensation of large background signal values. *Transactions of the institute of measurement and control*, 20:195–202, 1998.

[42] Slawomir Tumanski. Induction coil sensors—a review. *Measurement Science and Technology*, 18(3):R31–R46, mar 2007. ISSN 0957-0233. doi: 10.1088/0957-0233/18/3/R01.

[43] IEEE International Committee on Electromagnetic Safety. IEEE C95. 1-1992: IEEE Standard for Safety Levels with Respect to Human Exposure to Radio Frequency Electromagnetic Fields, 3 kHz to 300 GHz. *IEEE Standards*, 2005.

[44] International Commission on Non-Ionizing Radiation. ICNIRP Guidelines for Limiting Exposure to Time-Varying Electric, Magnetic and Electromagnetic Fields (up to 300 GHz). *Health Physics*, 74(4):494–522, 1998.

[45] O.C. Zienkiewicz and R.L. Taylor. *The finite element method, The basis*, volume I. 2000.

[46] D K Cheng. *Field and Wave Electromagnetics*. Addison Wesley, 2nd edition, 1989. ISBN 0201128195.

Chapter 3

Mathematical models based on FEM

3.1 Geometry and modelling

Although cardiac cycle, heart activity and breathing mechanisms affect several organs, as stated before, our hypothesis is focused on the conductivity changes in lungs and heart during the respiration and beating cycles, so for simulation reasons, the thorax was considered as the main area of interest.
Before solving the problem in FEM software, thorax should be modelled and imported to COMSOL (or to be designed within COMSOL). The alternatives to do so were to use a CT of human thorax developing a complete and complicated model, to draw and design a simplified one with CAD software or as stated before, design a simple model within COMSOL.

3.1.1 Thorax modelling using Computed Tomography scan

Thorax is a complicated multilayer structure and not easy to model. Using Computed Tomography or Magnetic Resonance images could help developing a 3D model of lungs, heart and other important organs of thorax cavity.
Although it might sound as an ideal method, it is difficult enough not to be used

by the majority of researchers and engineers who are looking to simulations as a tool to estimate the results ranges. For modelling using CT or MRI, one should go through segmentation process which is an area of research on its own.
It should be considered that the output model of such a conversion should be compatible with the FEM software import module and the related simulation parameters. Two tools we have found useful for this conversion are 3DSlicer [1] and Simpleware [2].

3.1.1.1 3DSlicer

Slicer or 3DSlicer is a free, open source software package for visualization and image analysis. It's a research package and initiated as a master project between surgical planning laboratory at the Brigham and Women's hospital and the MIT Artificial Intelligence Laboratory in 1998.
The latest version is released in July 2015. however, at the simulation stage of this thesis, an older version was tried.
Construction and Visualization of MRI, CT data were the first objectives of this software so for making the 3D output model compatible with a FE software, few experience were (and are) available.
Complicated structure of thorax results in crashes of software while re-sampling and make it very difficult to obtain a good quality segmented model free of discontinuities or black points.[1]
Although, finally it was decided not to use this software for converting the CT/MRI files, its worth mentioning that 3DSlicer is an open source and free software which enables us as students to learn a lot about the basics of modelling and image analysis. Figure 3.1 shows the dashboard of the program.

3.1.1.2 Simpleware

Simpleware is a 3D image processing, analysis and model generation software. It provides tools for converting 3D image data into computational models for biomedical analysis and generate meshes for export to FE solvers. The final 3D model could be exported as volumetric mesh, COMSOL model or COMSOL

[1] In segmentation black points are points which are very close to the background color and cause discontinuities in the final model

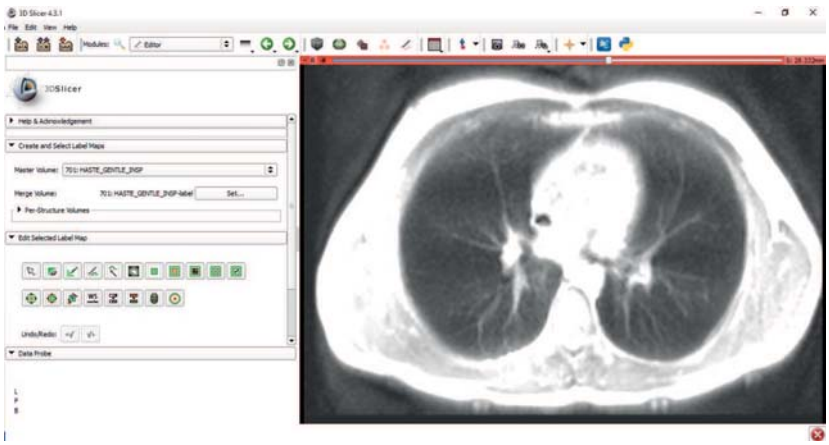

Fig. 3.1 3DSlicer dashboard with a CT scan of thorax loaded

mesh. It also provides several other output formats which are compatible with ANSYS, Solidworks, etc.

The program is not free nor open source but upon request, a one-month trial version is available for research centres and universities. Simpleware is a relatively new and few similar problems have been solved by this software to be used as a reference.

Despite 3DSlicer, Simpleware is a very powerful user-friendly software for re-sampling, segmentation and conversion medical images. On the other hand, when it comes to COMSOL there are some problems/incompatibilities which to the knowledge of the author, are mainly due to limitations of COMSOL and were not solved until version 4.4 of COMSOL, some are listed here:

- COMSOL imports the model as a finalized mesh. It's not possible to add any other components later (e.g. coils in our case) which is a familiar problem importing models from Solidworks or 3DSlicer.
  In fact this is an issue of COMSOL, because up to version 4.4 of COMSOL, Boolean operations (i.e. Union) on geometries created from mesh (like STL, VRML, etc.) were not supported.

- Simpleware +CAD module could be used to work around these limitations, designing the whole geometry (coils and thorax) in Simpleware, but a new problem arises. In FE solver, it might be necessary (depends on the type

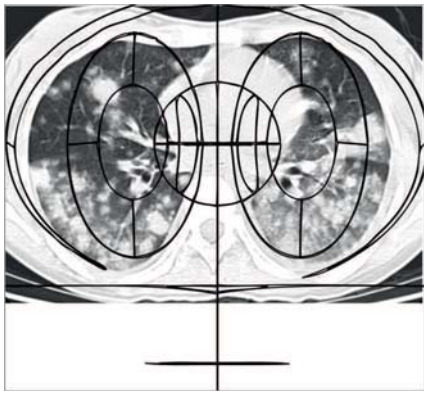

Fig. 3.2 Top view of the model

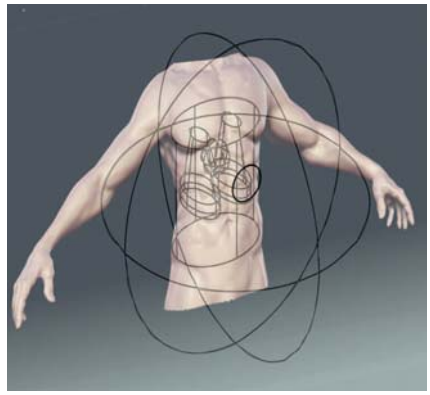

Fig. 3.3 General view of the model

of solver) to define reference edges or edge boundary conditions. COMSOL do recognize the domains and sub-domains of the imported model/mesh, but not edges.

Due to the mentioned problems, we finally decided to design and model the whole system within COMSOL to avoid later incompatibilities. A simplified 3D model of the human trunk (including lungs and heart) was designed within COMSOL. A current carrying coil is located in front of the chest as an excitation coil. Various simulations have been performed and different parameters were studied which will be explained in the next sections.

3.1.2 Thorax modeling in COMSOL

The main model consists of a sphere as the surrounding area, a cylinder for trunk structure and cones and spheres for lungs and heart. A current carrying coil is located in front of the chest as excitation coil (figures 3.2, 3.3 and 3.4).

Since in magnetic induction, it is believed that the magnetic fields are not blocked by poorly conducting tissues such as bones [3], the model does not consist of ribs and other poor conductive parts of thorax to reduce the complexity of the resulted mesh.

The dimensions and volume of the designed organs are approximately the ones for a healthy normal male. Main tissue types used as material in the simulation, dielectric properties of the tissues at 10 MHz and the number of finite elements

of each organ are shown in table 3.1.
The applied Passive electrical properties of body tissues were derived from [4]. The application mode chosen was Magnetic Fields (mf) in the AC/DC module. The AC/DC Module provides an environment for simulation of AC/DC electromagnetic in 2D and 3D.
The AC/DC Module is a powerful tool for detailed analysis of coils, capacitors, and electrical machinery. With this module, we run a quasi-static simulation in Magnetic Field interface mode.

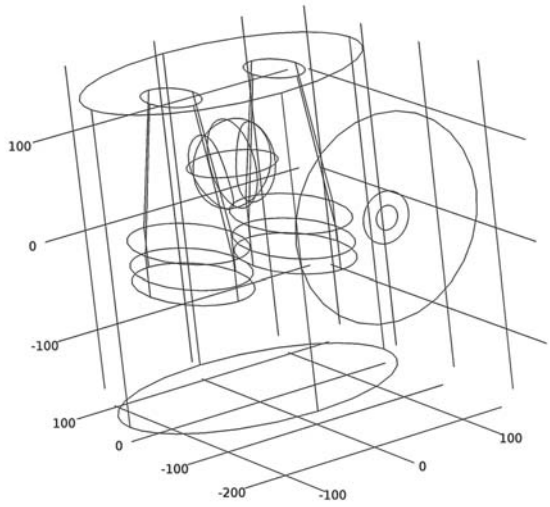

Fig. 3.4 The final model in COMSOL

The coils for excitation and detection (figure 3.5) were simulated as edge instead of toroid to avoid the necessity of small elements generation inside the coil domains. The excitation current was applied to the coil as boundary condition (1 Ampere).
The excitation coil has a radius of 25 mm and the detection (receiver) coil's radius is 100 mm and both are placed at a minimum distance of 10 cm from the chest. Coil design procedure, configuration, optimization and the electrical safety simulations will be explained in detail in chapter 4.

Table 3.1 Number of elements and dielectric properties at 10.7 MHz (Operating Frequency)

Tissue	Number of elements	Conductivity S/m	Relative Permittivity
Muscle	30586	0,6	170
Heart	2847	0,4	293
Lungs inflated	7484	0,22	123
Lungs deflated	7484	0,44	180

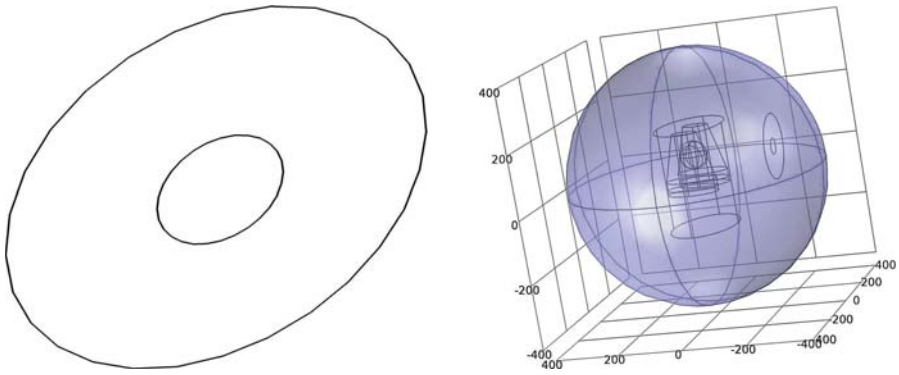

Fig. 3.5 Exc-Det coils

The next consideration in the simulation is the mesh elements and their size. The Mesh features enable the discretization of the geometry model into small units of simple shapes, the *mesh elements*.
The mesh generator discretizes the domains into smaller intervals. The endpoints of the mesh elements are called *mesh vertices*. The boundaries (or vertices) defined in the geometry are represented in the mesh by boundary elements.
Since our model is a 3D model, the mesh generator was able to discretize the domains into tetrahedral, hexahedral, prism, or pyramid mesh elements which we have chosen the free tetrahedral mesh elements (figure 3.6), with the default fine size. However, for different scenarios, we have switched to other available mesh features or changed the mesh element sizes in order to solve the equations.

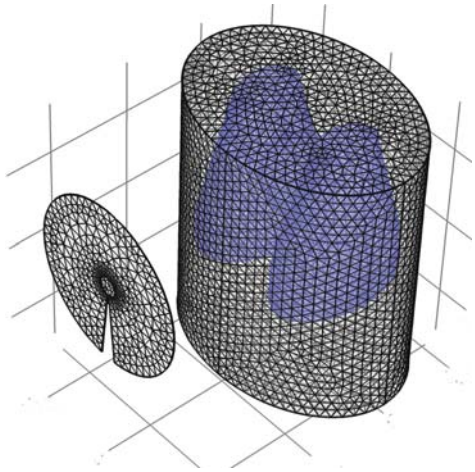

Fig. 3.6 Discretized domains into tetrahedral mesh elements

3.2 Electromagnetic field measurement simulations

As explained before, the perturbations caused by placing a conductive object in a time varying magnetic field is reflected in the imaginary part of equation 2.9. In order to measure the flux density, there are two alternatives, the straight way is to work with the imaginary part of the magnetic field. When nothing is placed in front of the coil (free space), the imaginary part is zero since no current is induced, while having even a low conductive object would cause a perturbation. The induced flux density (secondary magnetic field) can be calculated by integrating the orthogonal component of the magnetic field over the surface of the receiver coil.

$$\text{Induced flux density} = \int\int_S mf.(B_0 + \delta B) \tag{3.1}$$

3.3 Frequency dependency

In biomedical magnetic induction systems (especially tomography systems), in an attempt to increase the size of the secondary signal, higher frequencies than the industrial tomography (up to 500 kHz) have been used.
The accessible frequency range will extend from several tens of kHz up to tens of MHz, in which the upper limit is determined by the penetration depth of the

electromagnetic field and the desired sounding depth [5].
Using the specifications and methodology described before in this section, the secondary magnetic field was measured in various frequencies by simulations. The impact of inflation and deflation of the lungs was added by changing the conductivity of the lungs in each mode (figure 3.7).
Here in this simulation, the distance between the coil and the body is 5cm. The dotted lines are the induced magnetic field values while the lungs are inflated. Since the conductivity is lower in this mode, the induced magnetic field is smaller than in the deflation mode.

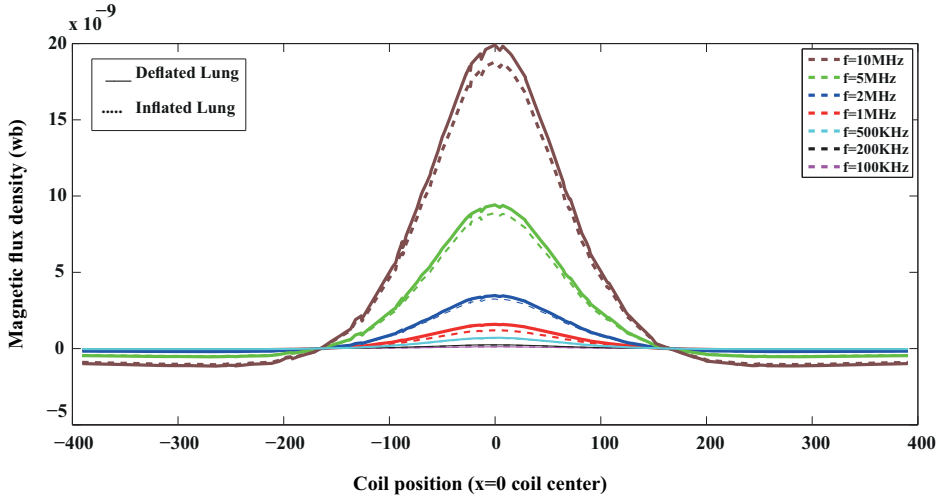

Fig. 3.7 Secondary magnetic field vs. frequency

3.4 Exposure simulation

For simulating the SAR, parametric sweep study node has been used to find the solution to a sequence of stationary or time-dependent PDE problems.
Frequency and the space between the excitation coil and the body were defined as variables in order to study the effect of those parameters on SAR and determine a safe margin of distance and frequency for the system. Based on the definition of SAR mentioned before, the following formula was used to calculate SAR in

COMSOL.
In this equation (3.2), $mf.QH$ is the electromagnetic heating averaged over the density of the tissue. Both deflating and inflating modes of lungs were considered in the simulations and the conductivity of tissues was also swept to be in accordance with frequency dependence state of conductivities.

$$SAR = mf.Qh/rho(trunk) \tag{3.2}$$

The studied frequencies are 100 KHz, 200 KHz, 500 KHz, 1 MHz, 2 MHz, 5 MHz and 10 MHz and the distance between chest and the excitation coil varies from a minimum of 5cm to 20cm with 5cm steps.

3.4.1 Results and conclusions

Figure 3.8 shows the SAR simulation results. The estimation of the absorption rate at the mentioned frequencies and distances shows that even considering the worst case for exposure to the magnetic field (a frequency of 10 MHz and 5cm distance), the maximum SAR is orders of magnitude lower than the safety standards' limits.
That is, for an excitation current of 1 A in a one turn coil at a distance of 5cm from the chest at a frequency of 10 MHz, we are more than one order of magnitude under the safety limits imposed by ICNIRP standard (maximum calculated SAR=0.0056 W/Kg).

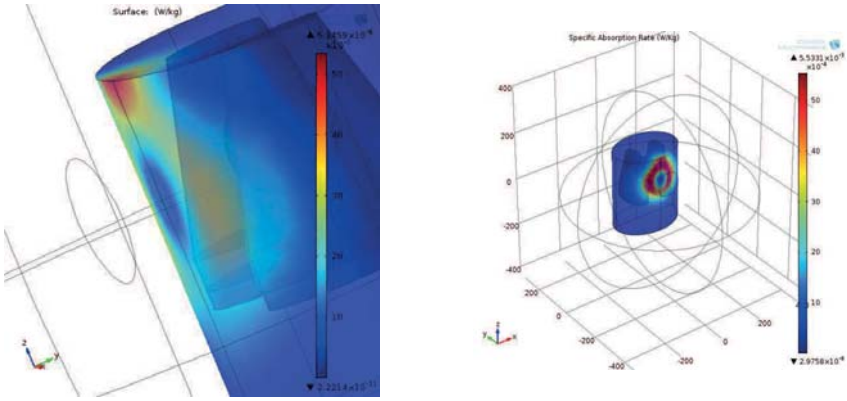

Fig. 3.9 SAR simulation results at 1 MHz (left) and the worst case (10 MHz-5cm)

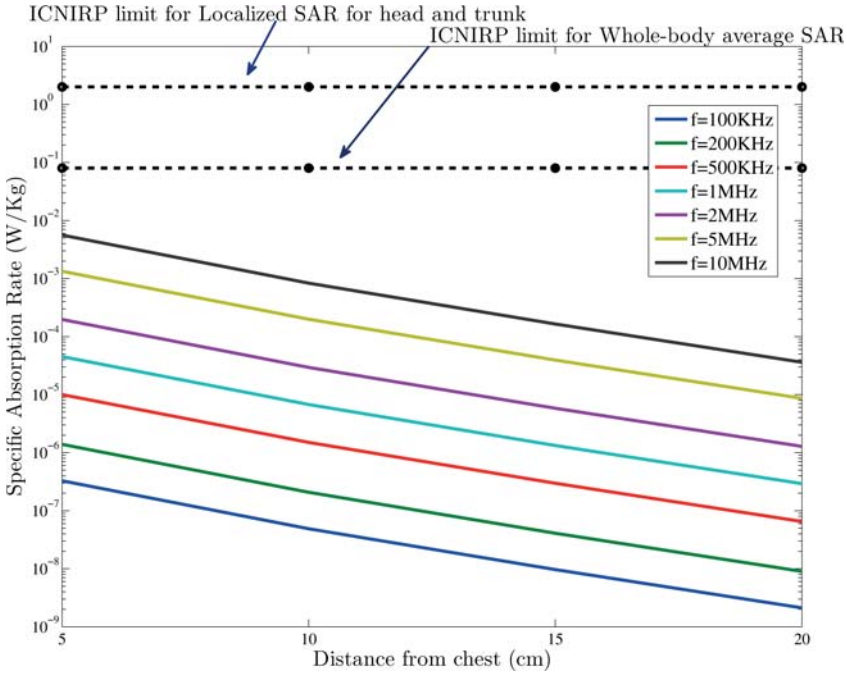

Fig. 3.8 SAR vs. distance of Exc coil from chest

References

[1] 3D Slicer. URL http://www.slicer.org/.

[2] Simpleware Software. URL https://www.simpleware.com/software/.

[3] H Griffiths, W.R. Stewart, and W Gough. Magnetic Induction Tomography: A Measuring System for Biological Tissues. *Annals of the New York Academy of Sciences*, 1999.

[4] C Gabriel, S Gabriel, and E Corthout. The dielectric properties of biological tissues: I. Literature survey. *Physics in medicine and biology*, 41(11):2231–49, nov 1996. ISSN 0031-9155.

[5] H Scharfetter, H K Lackner, and J Rosell. Magnetic induction tomography: hardware for multi-frequency measurements in biological tissues. *Physiological Measurement*, 22(1): 131–146, 2001.

Chapter 4

System Design and Implementation

4.1 MI system with adjacent coils

4.1.1 System description

The first designed MI system, was mainly to test the receiver design and had two coils for excitation and detection placed adjacently and a demodulation system based on PXI-5122. The excitation signal came from a 16-bit arbitrary waveform generator (PXI-5422, National instrument) operating at a sample rate of 200 MS/s. The signal received at the detector coil was passed to a two stage low noise amplifier (AD8432) with a gain of 64. The amplified signal is then, sampled at 100 MS/s by a 14-bit digitizer (PXI-5122, National Instruments). The driving frequency for the measurements was fixed to 10 MHz. In this configuration, the coils are two 8-turn coils with a diameter of 5 cm (figure 4.1) that could be placed on a common printed circuit board (PCB).

The generator (PXI-5422) has been configured to produce a sine wave with a desired frequency and amplitude as excitation signal with an injected current of 22 mA. The signal at the detection coil (RX) is then passed through the AD8432 to be amplified to the input level of the digitizer. The amplifier is an AD8432 which is a dual channel, low power amplifier with an input voltage noise

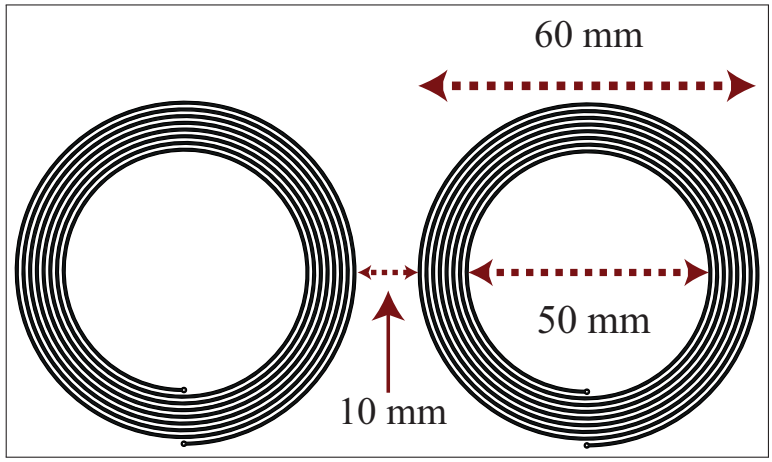

Fig. 4.1 EX-RX coils configuration,

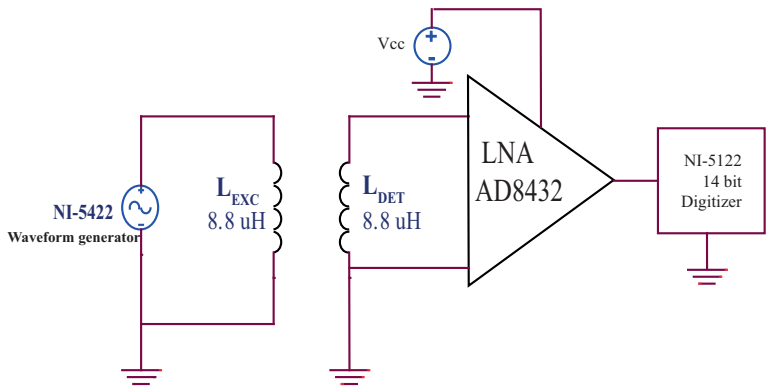

Fig. 4.2 Block diagram of an adjacent coil structure MI system

of 0.85 $nV/\sqrt{Hz}$. Both channels of the amplifier are set to a gain of 18.06 dB (×8) providing a total amplification of ×64, driven with a single-ended input and measured unipolar at the output. Figure 4.2 shows the block diagram of the described system.

4.1.2 Measurement protocol

Six saline solutions, in plastic tanks of 8 liters and dimensions of 30X15X15, were made up with conductivities of 0.0005, 0.2, 1, 2, 5, 16 $[Sm^{-1}]$. The experiment steps are as follows; place the tank at a distance of 5 cm from the sensor's head, step back, wait for 3 seconds, step forward and touch the tanks for 2 seconds, step back, wait for 3 seconds more and finally take it out. For each experiment, 40 measurements have been done in 22 seconds [1].

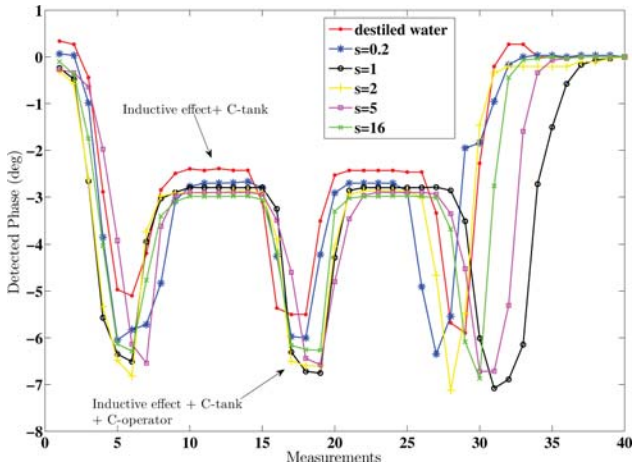

Fig. 4.3 Phase angle of the detected signal

4.1.3 Results and discussions

Equation (2.9) predicts that the imaginary component of the secondary magnetic field (ΔB) must be proportional to σ. The equation is valid when the skin depth of the electromagnetic field is much larger than the thickness of the sample.
As the conductivity increased, the skin depth became comparable to the diameter

of the tank, i.e. for a conductivity of 16 $[Sm^{-1}]$ the skin depth is 3 cm in comparison with 16 cm of tank diameter. The simulation confirms this issue and it can be seen in figure 4.4 that, there is a change in the slope for greater values of σ.

Moreover, figure 4.4 shows that we have an overestimation of the phase angle. When the operator is touching the tank, a phase change -from free space situation- of about 6° can be seen in the graphs (figure 4.3) while without touching, the maximum phase change is about 3°.

Although the phase was adjusted to the empty space case, these phase changes could still not be explained only by magnetic induction effects, and the capacitive coupling must play an important role that is in accordance with [2] and [3].

The changes produced when the user touches the bottles are not due to direct coupling between the object and the coils. It must be due to the direct coupling between the coils, object, and the ground through the user who is touching the bottle.

There are also measurement errors due to misplacement of the tank over the sensor. Experimentally, we obtained that a misplacement of 1 cm, in the same axis as cylinder's axis, produces a change of about 0.29° and a misplacement of 1 cm, in the axis perpendicular to the cylinder's axis, produces an approximate phase shift of 0.047°.

These phase changes could also be explained by capacitive coupling. As the capacitive effect is mainly related to the distance between the object and the coils, and magnetic induction is more sensitive to the changes in conductivity, we want to evaluate the possibility of using both magnetic and capacitive effects to monitor vital signs

The advantage of monitoring physiological signals is that they are rhythmic and the artifacts and unwanted static signals, produced by environmental factors, could be suppressed by signal processing techniques.

Based on the results of this experiment, we later changed the design of the coils to optimize the balance between capacitive and magnetic effects. A gradiometer structure (APG) was then applied as a field cancellation method to suppress the large primary magnetic field and increase the sensitivity of the magnetic induction signal.

Different topologies of gradiometers and coils suitable for being implemented on a PCB were studied and will be explained later in this chapter.

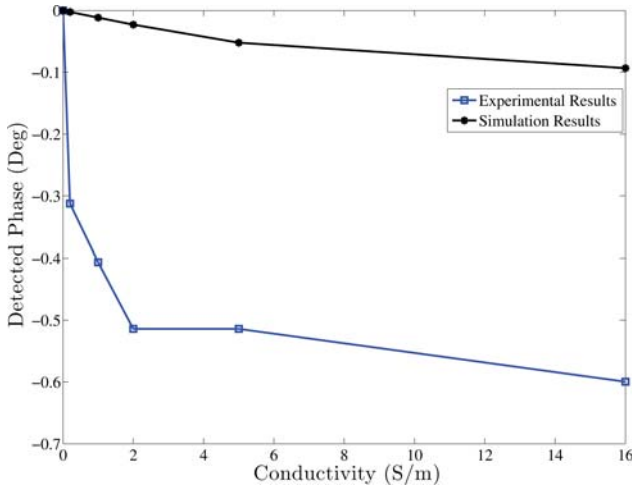

Fig. 4.4 Phase angle increment due to changes in σ

4.2 MI system with APG

As stated in chapter 2, in MI systems there are two contributions to the signal detected by the RX coil. The first is directly induced by the field from the excitation coil (TX) called the primary signal and the second is the eddy current induced within the object under study (desired secondary signal) [4].
The primary field signal is by some decades higher than the secondary signal of interest, and is responsible for introducing noise into signal measurements by two means— by restricting the gain which may be applied to the received signal and thereby increasing the contribution of quantization errors.
Gradiometers have been used in order to minimize the response to primary field signal in the receiver antennas. In this method, two sensor coils are placed at equal distances on either side of any axis of symmetry of to the excitation coil. The coils are then connected in serial opposition to produce a gradiometer [4].
Variations on this method include placing the sensor coil pair symmetrically about the plane of the excitation coil to produce an axial gradiometer and placing the

sensor coil pair symmetrically about the center axis of the excitation coil to produce a planar gradiometer [5][6].
This configuration is highly sensitive to the displacements and the zero sensitivity plane in the center of this structure is not desirable. Capacitive coupling has a higher impact on this structure and needs to be addressed.
To overcome these drawbacks and improve the level of the received signal, we studied different topologies of gradiometers as a field cancellation method to minimize the primary magnetic field while maintaining/ improving the sensitivity of the system to the induced desired signal.
The design of the new receiver antenna is partly based on the design explained in the patent application; "Coil arrangement for a magnetic induction impedance measurement apparatus comprising a partly compensated magnetic excitation field in the detection coil" [7]. Developing the idea described in the mentioned patent, the design process started from scratch and each and every step were first simulated by COMSOL with various assumptions. In the following sections, the design process will be described in detail.

4.2.1 System description

The system is based on two coils as excitation and detection coils and a phase sensitive detector. The excitation signal is provided by a signal generator at a frequency of $10.7 MHz$ because there are low-cost ceramic filters available at this frequency. The coils have been designed in a planar configuration and implemented in printed circuit board to be placed under the mattress.

4.2.1.1 Excitation coil

The excitation coil is an 8-turn spiral coil with an inner diameter of 5 cm implemented on PCB.
Based on the modified Wheeler formula [8][9] shown in equation 4.1, the self-inductance of the excitation coil is $6.93\,\mu H$. That is for an 8 turn spiral with wire diameter of $0.6\,mm$, turn spacing of $0.8\,mm$ and inner diameter of $50.84\,mm$. In equation 4.1, D_{avg} is the average coil diameter and the coefficients K_1 and K_2 are layout dependent.

The measured self-inductance of the coil (with HP4192A impedance analyzer) however, is $8.8\,\mu H$. The difference comes from the equation's approximations and layout dependent coefficients.

$$L = K_1 \mu_0 \frac{N^2 D_{avg}}{1 + K_2 \varphi} \tag{4.1}$$

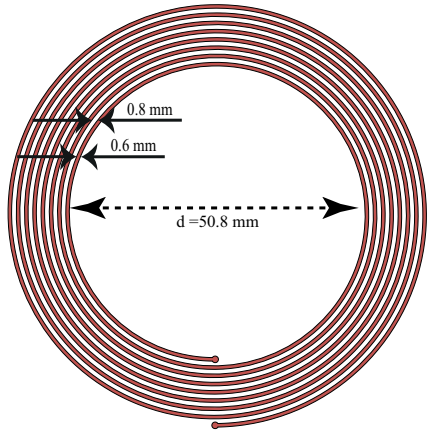

Fig. 4.5 Excitation coil final design

4.2.1.2 Receiver coil, APG

The APG is a one-turn antenna with a total measured inductance of $1\mu\,H$. This coil has a particular shape that is adapted to cancel out the primary field.
Similar to the excitation coil, the APG is implemented on PCB, located symmetrically (concentric) to the excitation coil. The separation between two coils is 2 mm and the outer section's radius of APG is 100 mm.
Through simulations, cancellation ratio and the optimum radius for APG were calculated to ensure and validate the design.

Cancellation ratio

Two set of simulations were performed in order to calculate the cancellation ratio (at free space and in the presence of the object, with and without cancellation).

In addition, parametric solver was used to resolving the APG's inner section radius where the cancellation is at maximum.
The object is the body model with the conductivities mentioned in table 4.1. The conductivity applied to the lungs is for the deflated mode.
The first simulation was performed with a one turn excitation coil and a one turn simple receiver coil (without any cancellation surface), placed concentrically.

$$\int_{S}\int \vec{B}_0.d\vec{s} - \int_{S_1}\int \vec{B}_0.d\vec{s} = 0 \tag{4.2}$$

The simulation then was repeated with the same excitation coil but a different receiver. The new receiver coil has a second surface acting like a second receiver coil which is connected in series to the first one.
To find the optimum radius for the inner circle of APG (inner coil), the radius of APG -outer area; S- was maintained as 100 mm and the radius of the inner surface (S_1) swept as a variable parameter. The parameter values were started from 1 mm up to 25 mm (the radius of the excitation coil).
Based on the gradiometer's principle, the excitation field in the first and second detection coils is cancelled by currents induced in the first and second detection surfaces adding up to zero (equation 4.2). The optimum radius for maximum cancellation calculated as 11.87 mm.

Table 4.1 APG Simulation's assumptions

Frequency		10	MHz
Object's distance from the sensors		50	mm
Object conductivity	Lungs	0,44	S/m
	Heart	0,5	S/m
	Muscles	0,6	S/m
Exc coil radius		25	mm
Det outer radius		100	mm

As explained before and according to the equation 2.3, the effect of primary magnetic field (B_0) appears in the real component of the detected signal. Comparing the results of APG simulation with the case of a simple coil for detection,

a cancellation factor of 5 orders of magnitude in the background signal could be observed.

On the contrary, the imaginary part of the signal (see table 4.2) which is the contribution of the eddy currents, experiences fewer changes after cancellation and stays at the same level of magnitude. The residual real part remained after applying the cancellation is the contribution of object's permittivity.

Table 4.2 APG simulation results

Radius	Simulation Description	Measured flux (Wb)	Measured Voltage (V)
R=100 mm, r= NA	No cancellation, No object	$1.21E^{-08} + 0i$	$0.76 + 0i$
R=100 mm, r= NA	No cancellation, with object	$1.23E^{-08} - 8.83E^{-11}i$	$0.77 - 0.0055i$
R=100 mm, r=11.87 mm	APG, No object	$1.09E^{-13} + 0i$	$9.25E^{-06} + 0i$
R=100 mm, r=11.87 mm	APG, With object	$1.78E^{-10} - 8.59E^{-11}i$	$0.011 - 0.0054i$

Figures 4.6 and 4.7 show the simulation setup.

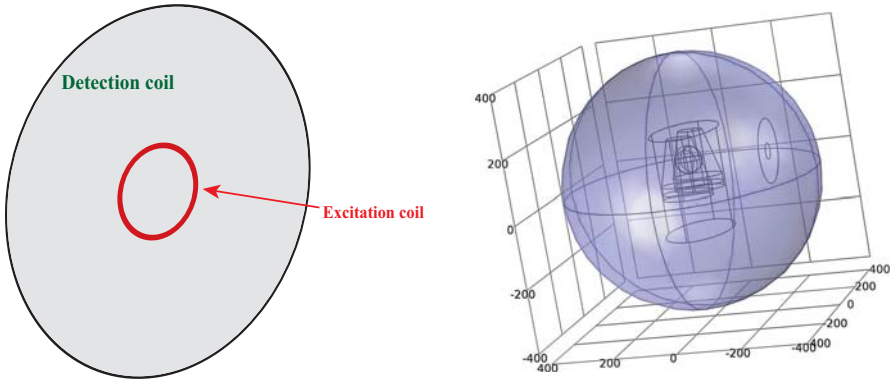

Fig. 4.6 TX-RX coils, no cancellation

Simulations were repeated with an 8-turn excitation coil (figure 4.8) and as expected, similar results were obtained.

However, the results from simulations will face some practical limitations in the implementation phase. The connections and capacitive coupling between wire lines are some of the important points which have to be considered in the hardware implementation.

An example of this practical limitations is shown in figure 4.9. In this design the capacitive coupling between two vertical lines of APG was high because of the

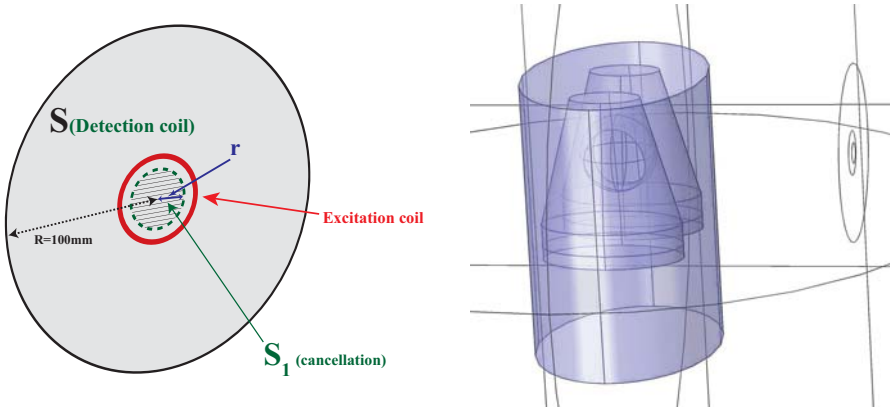

Fig. 4.7 TX-RX coils with the cancellation

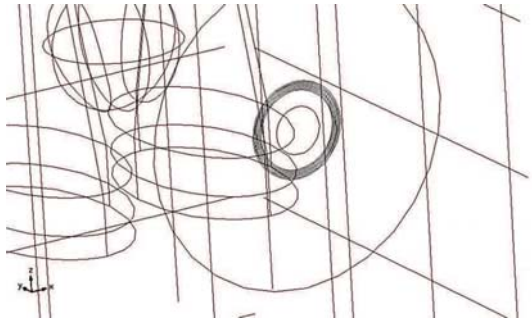

Fig. 4.8 Simulation model using 8-turn EXC coil, each turn carries a current of 1/8 A.

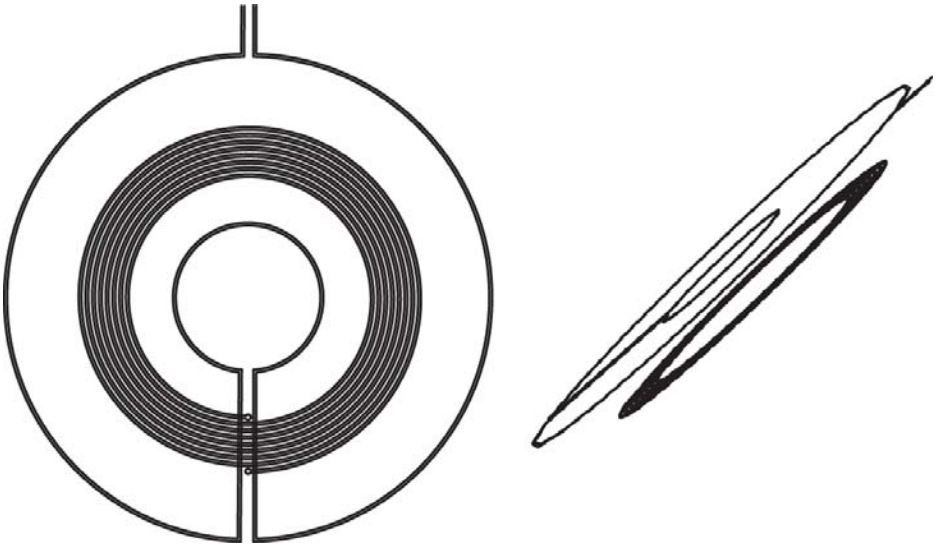

Fig. 4.9 a sample of tested configurations for TX-RX

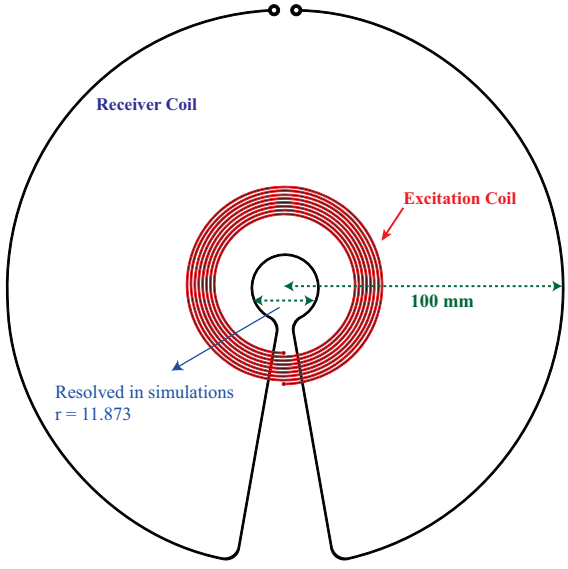

Fig. 4.10 TX-RX coils configuration, final design

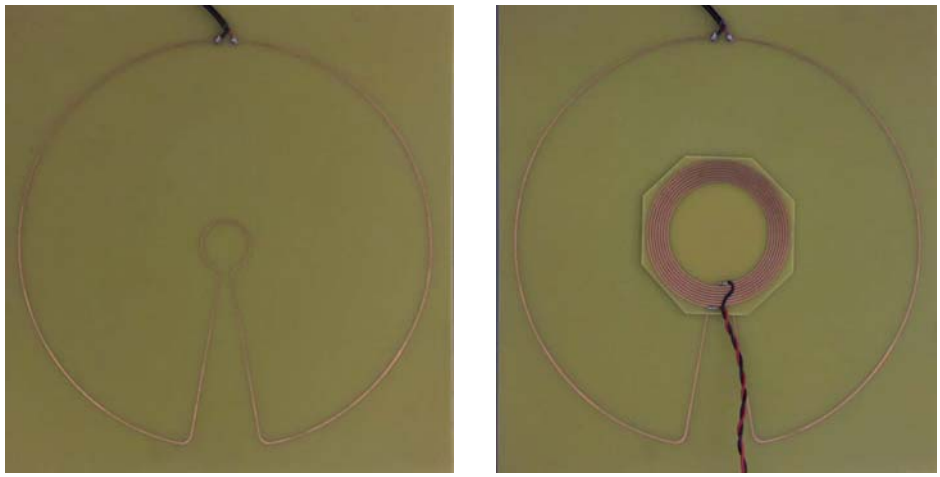

Fig. 4.11 The PCB implementation of the designed coils

proximity of the lines.
The measured inductance of the final PCB implementation of APG (4.10) is 1 μH. That is the total measured inductance of the coil. The analytical solution for inductance calculation gives a value of 0.55 μH for the outer section and a value of 0.07 μH for the inner section.
The difference between the analytical calculation and the measured inductance could be attributed to the gaps (opening section), equation's approximations and layout dependent coefficients.

4.2.2 Data Acquisition system

Given the small signals received by the APG, achieving the required phase measurement precision for vital sign monitoring application is a major challenge. An important component of an MIS is the amplifier and acquisition system which should be phase-stable and low noise.
In addition -as our objectives imply- the whole system should be low-cost and easy-to-install (low complexity)for the users. These reasons together with other previously mentioned shortcomings of the first version of MIS, lead us to an improved design for the acquisition system.
The signal received at APG will be amplified by a two stage low noise amplifier

(AD8432) with a gain of 64 and an input voltage noise of $0.85nV\sqrt{Hz}$.
The amplified signal is then filtered by ceramic filters at 10.7 MHz before being introduced to a gain and phase detector. AD8302 is an RF/IF gain-phase detector with an accurate phase measurement scaling of 10 mV/deg, used for demodulation and phase detection.
The reason for using the ceramic filters is due to the fact that the AD8302 is not a coherent phase detector and is sensitive to the interference signals at other frequencies than the 10.7 MHz. In addition, phase sensitive detectors are slightly more expensive than the AD8302.
The excitation signal is provided by a signal generator at an operating frequency of 10.7 MHz. Figure 4.12 shows the block diagram of the developed system.
As a reference of the experiments[1], for breathing and cardiac activity signals, Pulse plethysmogram (PPG) and pressure transducer of a BIOPAC-MP36 system has been used to monitor and compare the signals detected by MIS and signals detected by different systems. The complete schematic of the implemented system (amplification and detection circuit) is shown in 4.14.

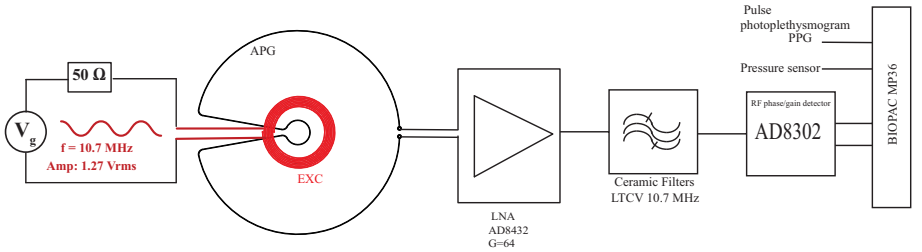

Fig. 4.12 MIS block diagram

The AD8432, is driven with a single-ended input measured differentially at the output. The unterminated bandwidth is 200 MHz. To achieve such low noise, the dual amplifier consumes 24 mA, resulting in a power consumption of 120 mW. The inverting input is ac-coupled to the ground with $0.1\mu F$ capacitor for proper operation and maintaining the internal dc bias levels.
R_{SH} and C_{SH} are resistor-capacitor shunt network (RC) to enhance stability at higher frequencies and reduce gain peaking and interference. General purpose

[1] Full description of the experimental setup will be provided in chapter 5.

pulse transformers[2] have been used at the output of each amplifier stage for isolation purposes (1CT:1CT), trying to suppress the capacitive coupling to the ground.
The LTCV10.7 filters (ceramic filters) are small, high performance chip filters consisting of 2 ceramic elements.
AD8302 measures the magnitude ratio (gain) and phase difference between two signals. Logarithmic amplifiers provide a logarithmic compression function that converts a range of input signal levels to a compact decibel-scaled output. In our design, AD8302 was configured in measurement mode. The mathematical formula of the chip acting in measurement mode is:

$$V_{MAG} = R_F I_{SLP} \log(V_{INA}/V_{INB}) + V_{CP} \tag{4.3}$$

$$V_{PHS} = -R_F I_{\phi}(|\phi(V_{INA}) - \phi(V_{INB})| - 90^{\circ}) + V_{CP} \tag{4.4}$$

V_{INA} and V_{INB} are two input signals which in our case one is the reference signal (same excitation signal) and the other is the output signal from the amplifier. For the gain function, $R_F I_{SLP}$ is 600 mV/decade. With a center point of 900 mV for 0 dB gain, a range of -30 dB to +30 dB covers the full-scale swing from 0 V to 1.8 V. For the phase function, the slope represented by $R_F I_{\phi}$ is 10 mv/degree. With a center point of 900 mV for 90°, a range of 0° to 180° covers the full scale swing from 1.8 V to 0 V. The range of 0° to −180° covers the same full-scale swing but with the opposite slope.

[2] 78615/2C, muRata Power Solutions

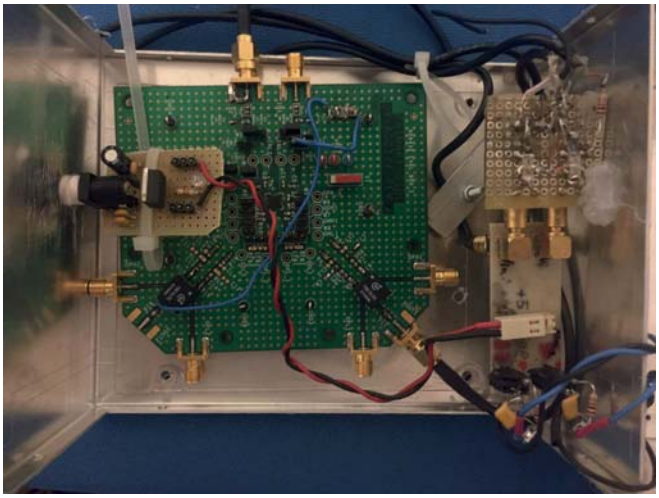

Fig. 4.13 Amplification and demodulation units (top view)

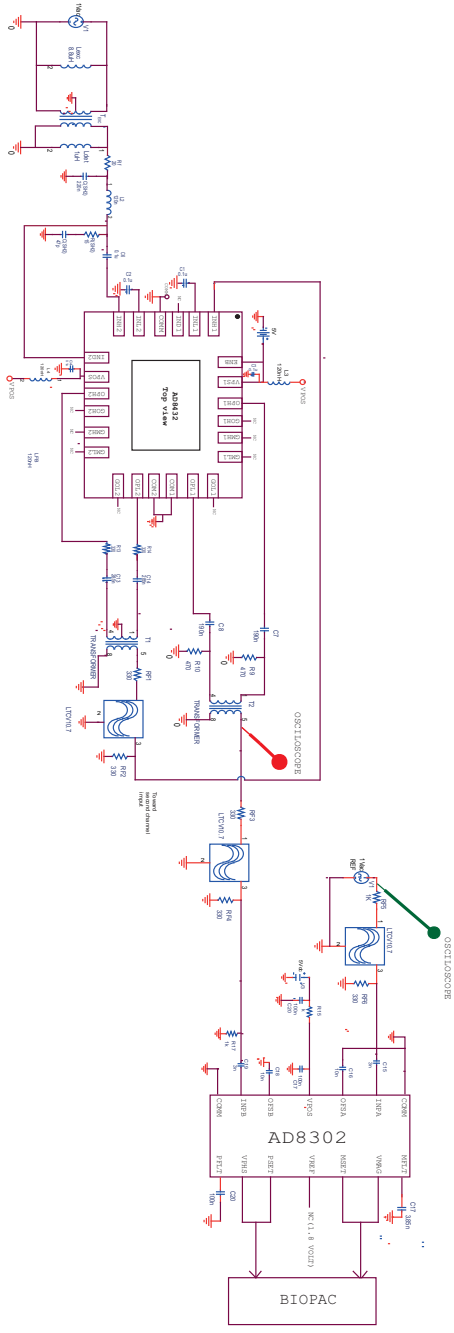

Fig. 4.14 Complete schematic of the developed magnetic induction system, signal amplification and detection circuits

4.2.3 Analytical system characterization

4.2.3.1 Mutual inductance

Considering two single-turn-co-planar, concentric coils of radii R_1 and R_2, with $R_1 \gg R_2$ shown in figure 4.15 the mutual inductance can be calculated as follows.

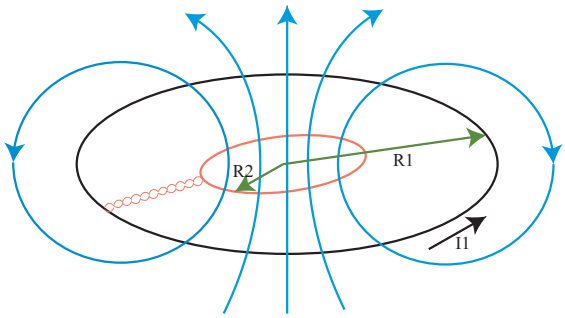

Fig. 4.15 Two concentric current loop

The magnetic field at the center of the ring due to I_1 in the outer coil is given by:

$$B_1 = \frac{\mu_0 I_1}{2R_1} \tag{4.5}$$

Since $R_1 \gg R_2$, we approximate the magnetic field through the entire inner coil by B_1. Hence, the flux through the second (inner) coil is

$$\Phi_{21} = B_1 A_2 = \left(\frac{\mu_0 I_1}{2R_1}\right) \pi R_2^2 = \frac{\mu_0 \pi I_1 R_2^2}{2R_1}$$

Thus, the mutual inductance is given by

$$M = \frac{\Phi_{21}}{I_1} = \frac{\mu_0 \pi R_2^2}{2R_1} \tag{4.6}$$

Based on equation 4.6, the mutual inductance calculated for different coil combinations are listed in table 4.3

Coupling coefficient

Common expression for the mutual inductance between two coils is given by equation 4.7. However, this equation assumes 100% magnetic coupling between the coils.
Practically, there is always some loss due to leakage and position. The amount of flux linkage can be defined as a fraction of the total possible flux linkage between the coils. This fraction value is called the coupling coefficient and is given as equation 4.8.

$$M = \sqrt{L_1 L_2} \tag{4.7}$$

$$K = \frac{M}{\sqrt{L_1 L_2}} \tag{4.8}$$

Using the previously calculated mutual inductance, the coefficients were calculated and are shown in table 4.3

Table 4.3 Calculated mutual inductance (M) and coupling coefficient (K) for EXC and APG

	Coils	Mutual inductance	Coupling coefficient
M12	Excitation coil & Outer coil of APG	118 nH	0.056
M13	Excitation coil & inner coil of APG	84 nH	0.1
M23	Two coils of APG	0.58 nH	0.003

Simulation

The mutual inductance between excitation and AP coils[3] were examined and computed using a frequency domain model in COMSOL (see figures 4.16 and 4.17).
A prescribed current of 1 A is flowing through a 8 turn coil of radius 25 mm (EXC), at the operating frequency (10.7 MHz). A 1 turn secondary coil with a radius of 100 mm, is concentric with the primary, and in the same plane. The wire radii in both coil is $r_0 = 0.6mm$. The coils are modeled in the 2D axisymmetric space, assuming no physical variation around the center line. Equation 4.6 is the main applied equation.

[3]The APG coils mutual inductance is negligible so was not included in the simulations.

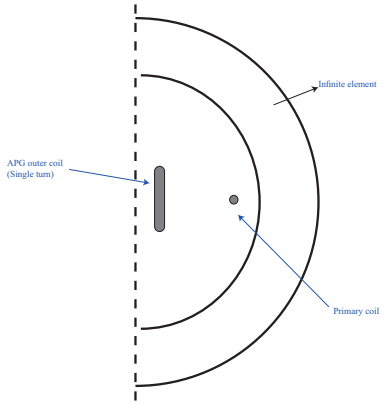

Fig. 4.16 Schematic representation of the 2D axisymmetric model of the EXC and APG (outer coil)

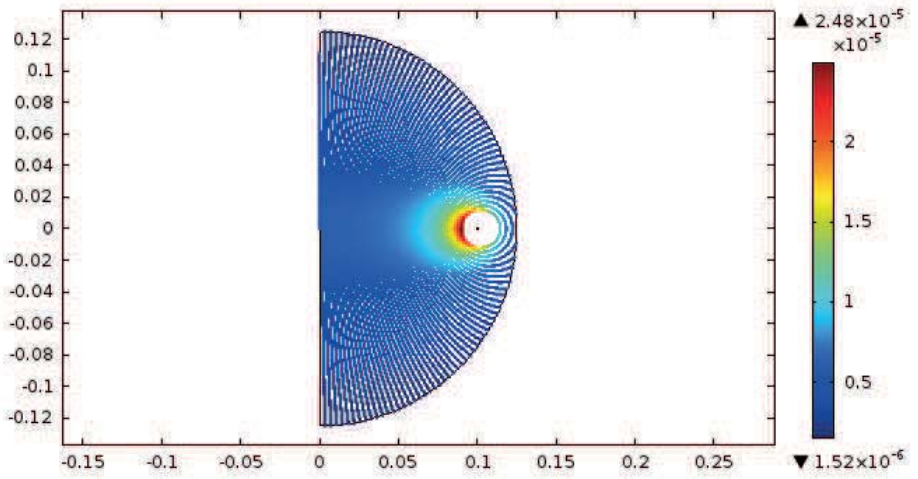

Fig. 4.17 Magnetic flux lines for the open circuit simulation

The results are in accordance with the analytical calculations; the mutual inductance between excitation and APG outer coil (bigger surface) is computed as 109 nH and an inductance of 0.65 μH for this section of APG.
The mutual inductance between excitation coil and APG inner coil is 48 nH, and the inductance of this APG section is computed as 0.048 μH. See table 4.3 for comparison.

4.2.3.2 Capacitive coupling

In an ideal magnetic induction (MI) system, the coupling between the object and the coils is expected to be only by the magnetic field. However, in a practical system, the electric field (capacitive) coupling also exists.
In the majority of the cases studied until now -especially in the applications in which the sample to be monitored (characterized or imaged) has low conductivity or is non-magnetic- it could be considered as an unwanted signal which causes large errors and makes the design of the system more complex.
In [10], the authors reported that the residual capacitive coupling affected mainly the real part of the signal and was therefore separated from the conductivity measurement by phase-sensitive detection, but [11] showed that the imaginary part could also be affected.
Since the received signal due to conductivity changes is very small, a small amount of contamination of the signal by capacitive coupling is important. In this section, the possible ways of signal contamination by capacitive coupling are studied.

Coupling mechanisms

The authors in [11], separated the coupling mechanisms existing in an excitation/detection pair of sensor coils, into six cases, two involving coupling directly between the source and the detector coils, and other four cases are related to coupling with the sample.

- Direct inductive coupling between the two coils (M_{12}), producing the large background signal of primary field at the RX coil. In order to subtract this signal, we have used a different design of receiver coil (figure 4.18).

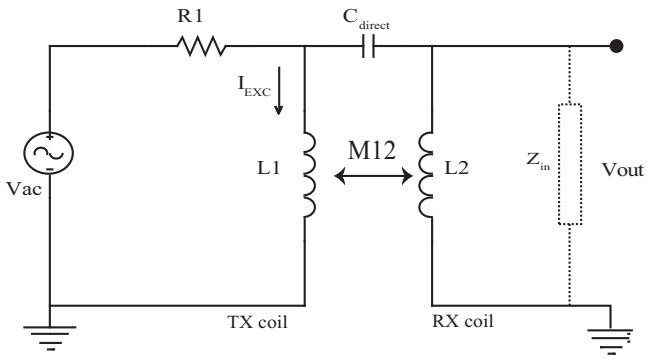

Fig. 4.18 Direct ind & cap coupling

- Direct capacitive coupling between two coils (TX/RX) through C_{direct}. This is the unwanted coupling and according to [11] is either in-phase or 180° out-of-phase with the primary inductive coupling (figure 4.18).

- Inductive excitation-inductive detection (M_{13}, M_{23}) which is the desired mode for detection of conductivity changes due to vital physiological activities of the body (figure 4.19a).

- Capacitive excitation-capacitive detection is again an unwanted effect caused by the potential difference between the exciter and the receiver through the object (figure 4.19b).
  The coupling is between the excitation and detection coils, through the object. The surface area of the object has a great impact in this coupling path. Losses associated with the resistance of the object will result in changes in the quadrature component of the detected signal, which can not be separated from the desired signal and so have to be minimized by precise grounding and screening [11].

- Inductive excitation-capacitive detection is an unwanted effect caused by voltages induced in the object by the magnetic field from the excitation coil, M_{13}. The object voltage is then could be detected through C_{23} (figure 4.20a) and C_{13_1} (figure 4.20b), it's difficult to quantify but it would be much smaller than the desired mode of coupling [11].

- Capacitive excitation–inductive detection is again an unwanted mode of coupling caused by the detection of the magnetic field created by displacement current through stray capacitance between the excitation coil and the object (figure 4.20b). This is supposed to be significant when the object and coils are of comparable size and close to each other [11].

Note that in figure 4.18 and the following figures "ind" stands for inductive and "cap" stands for capacitive.

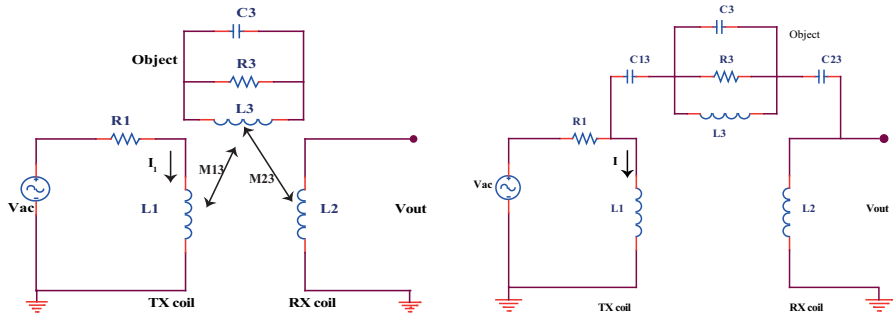

(a) Object's impact on ind-ind coupling

(b) Object's impact on cap-cap coupling

Fig. 4.19 Coupling paths and object's impact on these couplings (I), adapted from [11]

For the cross couplings and mainly to suppress the capacitive coupling, the main recommendation is to do the electrostatic screening. Screening may not necessarily improve the situation, especially for coils with a small number of turns because of voltages induced on the screen.
The screen is a large conductive area and may increase the parasitic coupling. It also could act as a single turn inductor and the EMF between one end of the screen and the other end will be 1/N times of the primary voltage (N=number of turns).
Comb screens can be used to screen the electric fields since they have little/no effect on the magnetic coupling. The cut lines do not allow the circulation of eddy currents but will screen the electric field. However, in small coils and in cases in which the object and the coils are very close, comb screening may not work either.
In our case, as we were looking for a practical and low-cost system and not for an *academic* version of the magnetic induction system, we decided not to

use screening. Our hypothesis is that the capacitive source in the signal will not cancel out the magnetic effect, and will produce a complementary source of information.

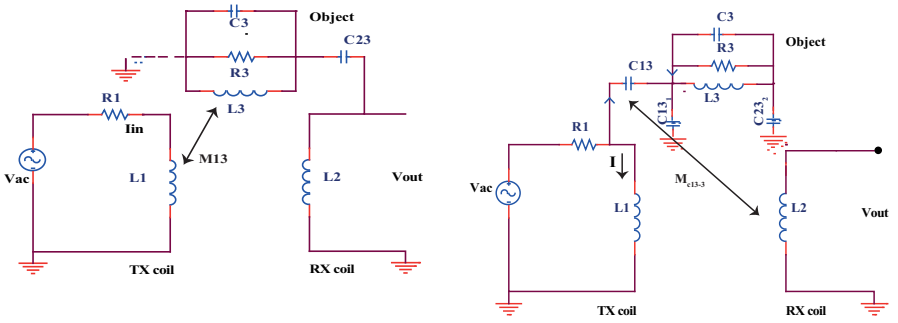

(a) Ind-cap cross coupling via object

(b) Cap-ind cross coupling via object

Fig. 4.20 Coupling paths and object's impact on them (II), adapted from [11]

Capacitance estimations using FEM simulations

Using the electrostatics study of COMSOL, we simulated the capacitance between the object and the coils and also between the coil planes.
The geometry and the model used in this section are similar to the previously described model, consists of two edge coils for excitation and detection. Excitation coil has a radius of 25 mm and the detection (receiver) coil's radius is 100 mm and both are placed at a distance of 5 cm from the chest. The chest, lungs and heart are designed with simple cylinders and cones.
The governing equations in the electrostatic simulations are:

$$\nabla.D = \rho_v \tag{4.9}$$

$$E = -\nabla V \tag{4.10}$$

where D is the electric displacement, E is the electric field, V is the electric potential and ρ is the electric charge density.
The results of the simulation are shown in table 4.4. C_1 is the capacitance between EXC and the object (body), C_2 is the capacitance between the APG and the object and finally the C_{21} is the capacitance between EXC and APG.

As expected, the capacitance between APG and the EXC is higher due to the proximity.

Table 4.4 Capacitance value calculated by electrostatic calculations

EXC-Body, C_1 (F)	**EXC-APG, C_{21} (F)**	**APG-Body, C_2 component (F)**
$-1.64E^{-12}$	$4.11E^{-12}$	$1.02E^{-12}$

These simulations provide us with the approximate capacitance values which later we used for modeling the circuit with ORCAD.

Direct capacitive coupling impact on primary field cancellation

As stated before in this chapter depends on the coupling coefficient and the adjustment of the coils regarding each other, a very small negligible residual primary voltage will remain at the output of the APG. However, the unwanted capacitive couplings affect the system including the primary cancellation.
We simulated the circuit with ORCAD to study the direct capacitive coupling impacts and the values obtained in the capacitive simulations with COMSOL. Using parametric simulations, different values of the direct capacitive coupling value were studied. In figure 4.21, the C_1 simulating the direct coupling as a variable capacitance taking the values of 4 pF, 2 pF, 1 pF, 0.1 pF, 0.01 pF and 0.001 pF. K_1 and K_2 are the coupling coefficients for the gradiometer-detection coils and the excitation-detection respectively.

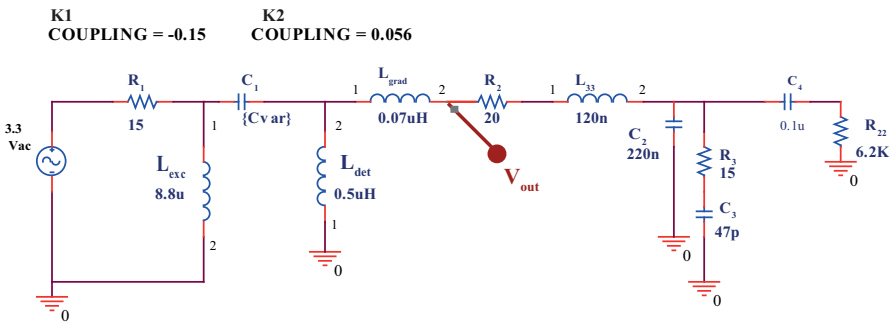

Fig. 4.21 Schematics for variable capacitance simulations

Parametric simulation results show that by increasing the C_1 value, the cancellation is faded and the residual voltage from primary field increases. Figures 4.22 and 4.23 illustrate the results.
Considering that the changes due to vital activities at the operating frequency are in the range of 10^{-4} to 10^{-6} [12], small increments in residual voltage alters/fades the desired signal and could cause wrong interpretation of the vital signals.

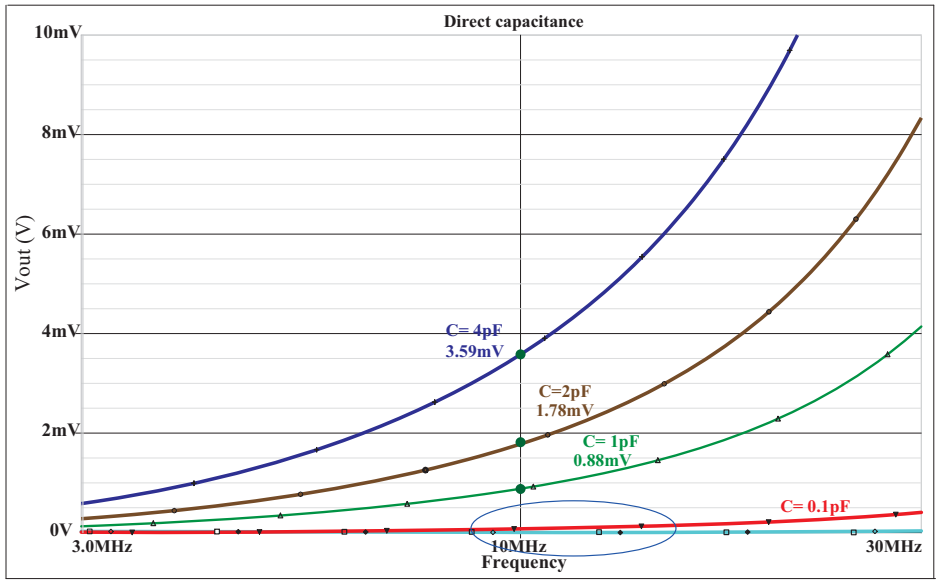

Fig. 4.22 Residual voltage due to different direct capacitance (I)

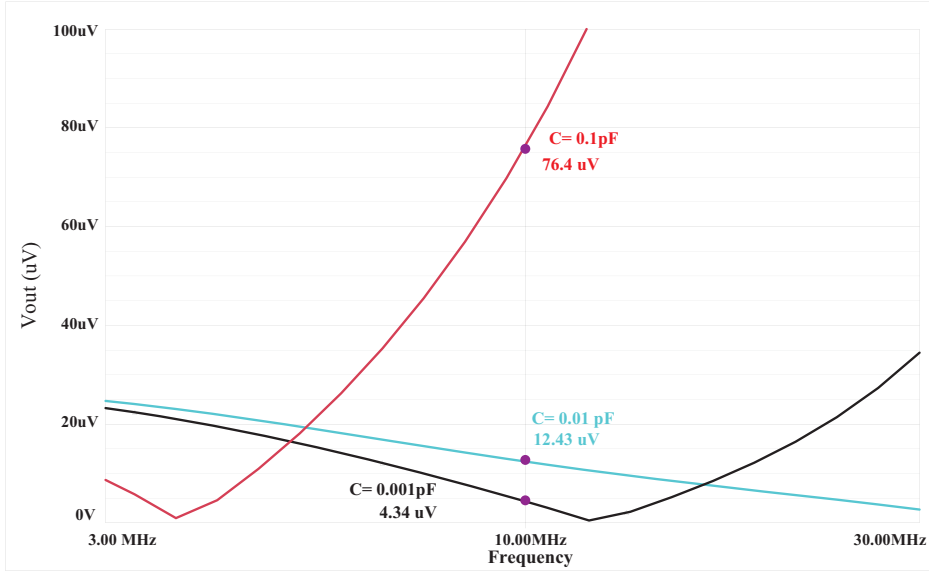

Fig. 4.23 Residual voltage due to different direct capacitance (II)

As explained previously, the magnetic field generated by the excitation coil results in eddy currents flow in patient's thorax, which re-induce a secondary field containing the information from thoracic area, a conductive part (R_{body}) and a capacitive part (c_{body}) that model tissue conductivity and permittivity (see equation 2.9).
The concept shown in figure 4.24 could be modeled in circuit representation illustrated in figure 4.25.

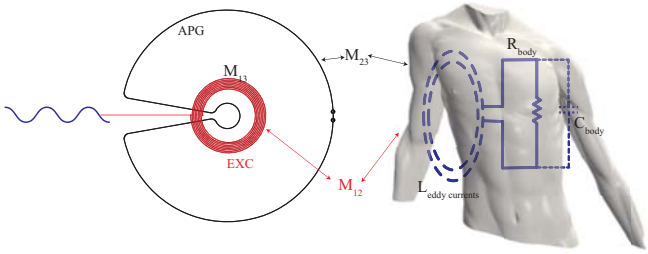

Fig. 4.24 Detection concept

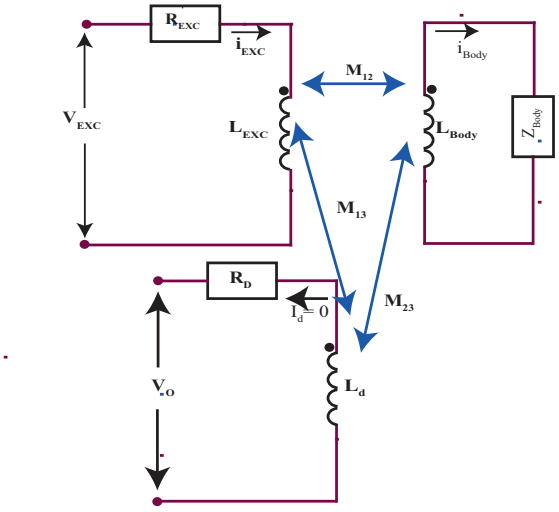

Fig. 4.25 Equivalent circuit of an excitation-detection coil pair

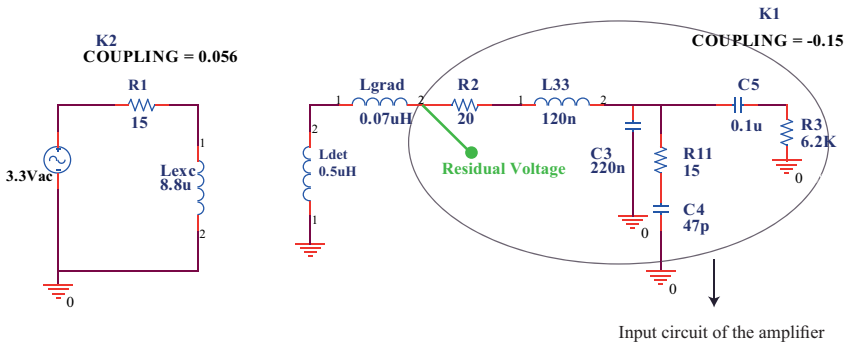

Fig. 4.26 Schematic of the MI circuit, adjustment simulations

In figure 4.26, L_{grad} is the inner part of APG and L_{det} is the outer section. The coupling coefficients (CC) used for the coils are estimated from the calculations previously explained. The coupling coefficient is a representation of the adjustment component.

It is crucial -for the system to work properly- to minimize this component in order to minimize the residual voltage and in analytical solutions we suppose the M_{13} to be zero or negligible.

Figure 4.27 shows the residual voltage for different values of adjustment (coupling coefficient between EXC and APG).

The minimum residual voltage (41.9 uV) obtained with a coefficient value of $K = -0.15$ between EXC and APG inner coil. As it can be seen for certain values of K, it is not possible to find a minimum close to zero for the residual voltage.

Figure 4.28 shows the frequency response of the system in the absence of the object.

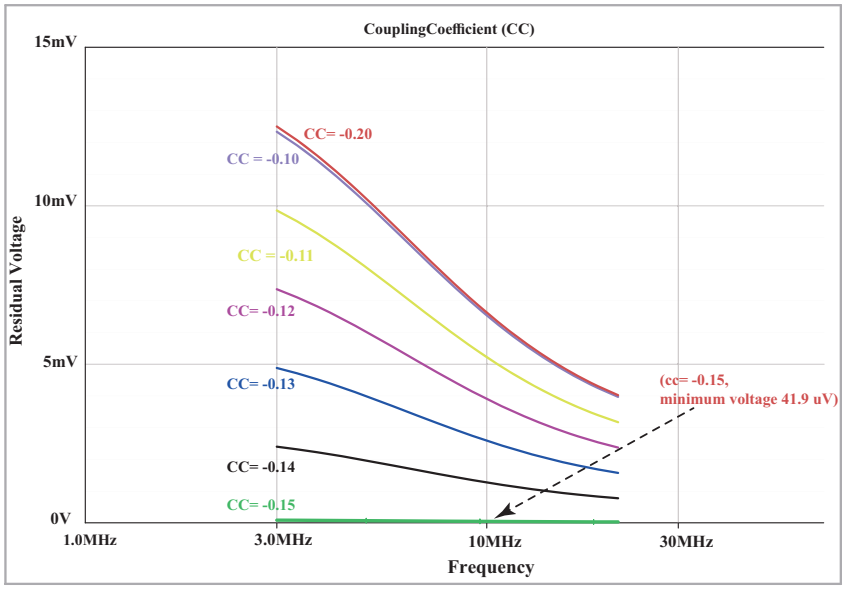

Fig. 4.27 Coupling coefficient (adjustment) impact on residual voltage at the output of APG

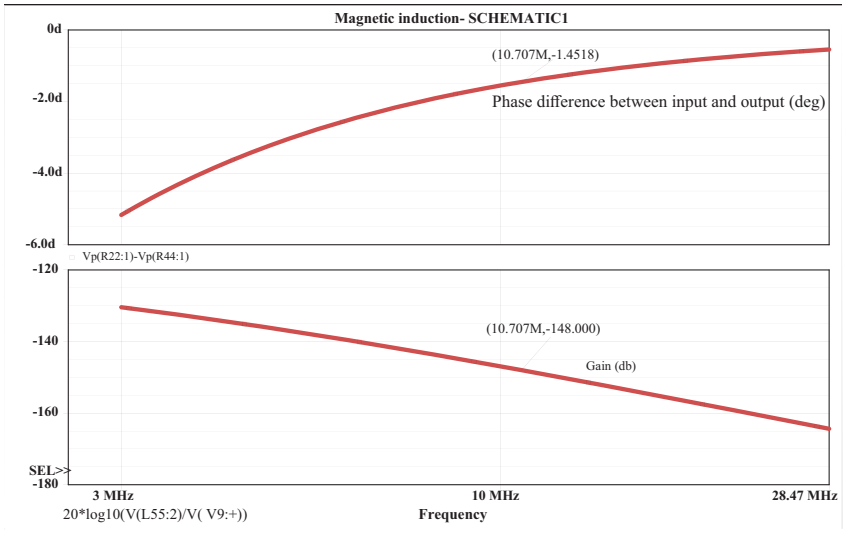

Fig. 4.28 Frequency response of the system in the absence of the object

4.3 Expected signal due to physiological activities

The secondary received signal at the detection coil is carrying the information of physiological activities. That could include breathing, cardiac activity, motions and other organ's contributions. In a series of simulations, we have simulated the breathing process. These simulations include conductivity changes of the lungs while inhalation/ exhalation of the air into/from the lungs, lung and thorax volume changes. Table 4.5 and figure 4.29 shows different scenarios for breathing simulations in order to find out the impact of each change on the signal and the results. Table 4.5 shows the measured secondary signal:

1. when the lungs are deflated (lower volume of air) and the conductivity and permittivity values are related to this state of the lungs. Distance from the chest is 50 mm. - Defl Nor

2. when the lungs are deflated (lower volume of air), the conductivity is the same as before (0.44 S/m) but the permittivity changed to inflation state permittivity (123). Distance from the chest is 50 mm. *Nor dEps*

3. when the lungs are deflated (lower volume of air), the conductivity changed to inflation state conductivity (0.22 S/m but the permittivity is the deflation related permittivity (180). Distance from the chest is 50 mm. *Nor dSigma*

4. when the conductivity and permittivity changes to inflation state related values (0.22 S/m and 123) but the volume remains as deflated (lower volume of air). Distance from the chest is 50 mm. *Inf no dV no dD*

5. when the lungs are inflated (higher volume of air) and the conductivity and permittivity values are related to this state of the lungs. Distance from the chest is 50 mm. *Inf dV no dD*

6. when the lungs are inflated (lower volume of air) with the associated parameters and volumes at a distance of 47 mm from the chest. *Defl dD*

7. when the lungs are deflated (higher volume of air) with the associated parameters and volumes at a distance of 47 mm from the chest. *Inf dV dD*

Table 4.5 Breathing simulations, different scenarios

Distance (D)	**Lung $\sigma(S/m)$**	**Lung ε**	**Lung Volume (l)**	**Flux density**	**Lung status, Changes**	**#**
50 mm	0,44	180	2,89	1,78 E-10 - 8,59 E-11 i	Deflated lungs	Defl Nor
50 mm	0,44	123	2,89	1,77 E-10 - 8,58 E-11 i	Deflated lungs, ε	Nor dEps
50 mm	0,22	180	2,89	1,79 E-10 - 8.03 E-11 i	Deflated lungs, σ	Nor dSigma
50 mm	0,22	123	2,89	1,78 E-10 - 8.01 E-11 i	Inflated lungs, ε ,σ	Inf no dV no dD
50 mm	0,22	123	3,45	1,78 E-10 - 7.75 E-11 i	Inflated lungs, $\varepsilon\,\sigma\,Volume$	Inf dV no dD
47 mm	0,44	180	2,89	1,86 E-10 - 8.86 E-11 i	Deflated lungs, D	Defl dD
47 mm	0,22	123	3,45	1,86 E-10 - 8.57 E-11 i	Inflated lungs, D and Volume	Inf dV dD

As the results suggest, reducing the permittivity from 180 to 123, produces a very low decrease in the real component and almost no effect on the imaginary component, while cutting the conductivity to half (from 0.44 to 0.23 S/m - as expected- cause a bigger change (7 percent decrease) in the imaginary component of the signal.

The simulations also showed that changing the conductivity together with the volume of the lungs from deflated to inflated mode, cause a 6.8 percent decrease in the imaginary component of the signal while the real component grows about 0.19 percent.

However, inhalation of air into the lungs produce a small increase in the thorax volume which could be considered as a small movement toward the sensors. An increase of 0.5 litre in thorax's volume, results in an approximately 3 mm displacement of the body toward the coils.

This modification in distance affects both components of the received signal. The imaginary component, in this case, decreases 0.21 percent changing from deflation to inflation mode while the increase in the real part of the signal is 4.3 percent. The impact of being 3 mm closer to the sensors is bigger than the impact caused by conductivity and permittivity changes.

The big change in the real component could be due to changes in the distribution of the currents at the surface of the object.

Figure 4.30 is a reproduction of figure 4.29 including zero flux, that better shows the various parameter changes and their impacts. It could be seen that the phase

angle does not change when the body approaches the APG and the imaginary part is reduced when lungs are inflated in this new position.

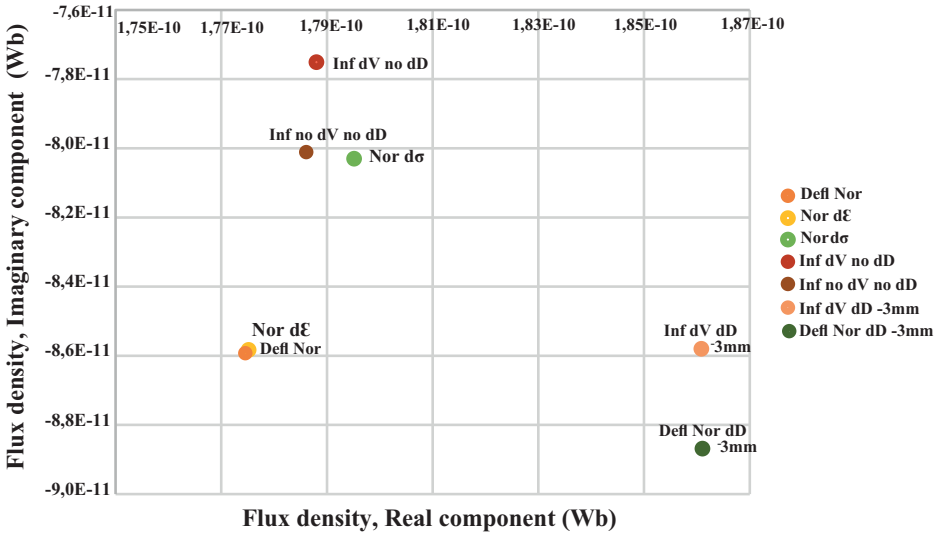

Fig. 4.29 Effect on the Imaginary and real part of the detected signal due to changes in different parameters related to breathing (I)

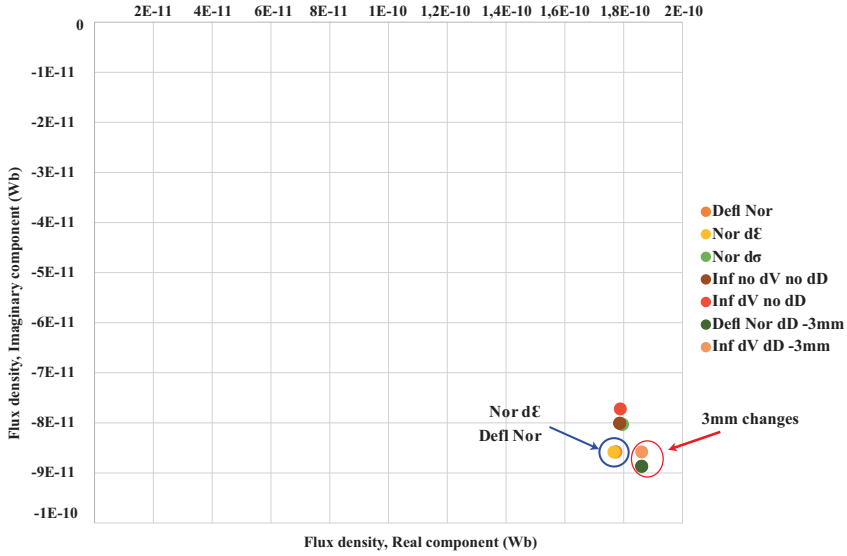

Fig. 4.30 Effect on the Imaginary and real part of the detected signal due to changes in different parameters related to breathing (II)

4.4 Sensitivity to position changes

The sensitivity of the system to the displacement of the object regarding the coils is simulated and studied in this section. That is to find the margin in which the system is still able to receive and detect signals from the physiological activities of the body. The assumptions used in these simulations are shown in table 4.6.

Table 4.6 Assumptions applied in the simulations of sensitivity to position changes

Frequency	10		MHz
Object's distance from the sensors	50		mm
Object conductivity	Lung	0.44	S/m
	Heart	0.5	S/m
	Muscles	0.6	S/m
X-axis displacement steps	20		mm
Z-axis displacement steps	10		mm

4.4.1 Horizontal sensitivity

Horizontal sensitivity means displacements of the object in regard to the coils and toward X axis (see figure 4.31). The displacement steps are of 20 mm and the sample has been moved 10 cm to the sides. Figure 4.32 and table 4.7 illustrates the results for horizontal sensitivity studies. According to the results (see table 4.7), by moving the object to the sides, both real and imaginary components fade but the imaginary component (secondary signal) decrease faster. Moving 8 cm to the sides causes a 41% reduction in the secondary signal while the primary field only reduces 25%. It could be concluded that, considering the dimensions of the coils in our design, an 8 cm margin for displacement to the sides could still be relatively sufficient to receive the information from the detected signal.

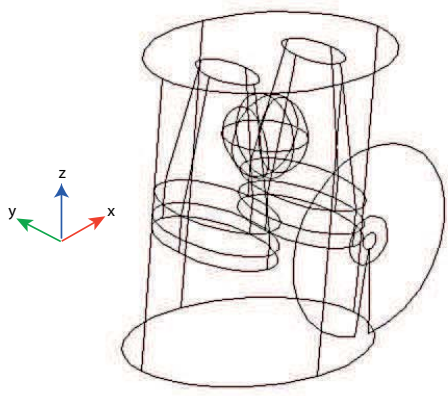

Fig. 4.31 Displacement direction for horizontal sensitivity studies

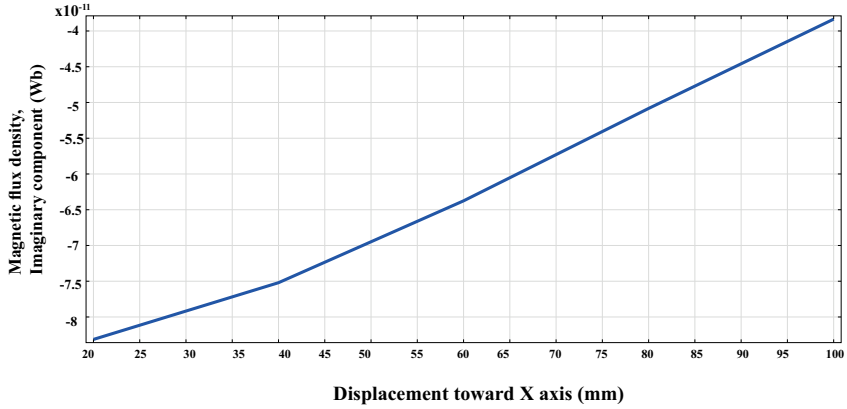

Fig. 4.32 System's sensitivity to displacement toward Z axis, imaginary component

4.4.2 Vertical sensitivity

Vertical sensitivity refers to the changes in the signal due to the displacement of the object along Z axis (figure 4.33). Since the model in this direction is not symmetric (as it was in horizontal simulations) the interpretation of sensitivity is complicated since other organs' contribution would be different in reality. Figure 4.34 and table 4.8 show the results. As the results imply, the displacement toward

Table 4.7 Magnetic flux density changes due to displacement toward X axis

Object displacement toward X axis (mm)	Magnetic flux density (Wb)
0	1,78 E-10 - 8,59 E-11 i
20	1.75 E-10 - 8.31 E-11 i
40	1.67 E-10 - 7.52 E-11 i
60	1.52 E-10 - 6.37 E-11 i
80	1.32 E-10 - 5.08 E-11 i
100	1.03 E-10 - 3.83 E-11 i

Z axis, both real and imaginary components of the signal are decreasing but similar to the displacement toward X axis, the imaginary component declines faster. By moving 50 mm, the imaginary signal decreases 41% while the real part decreases 36%.

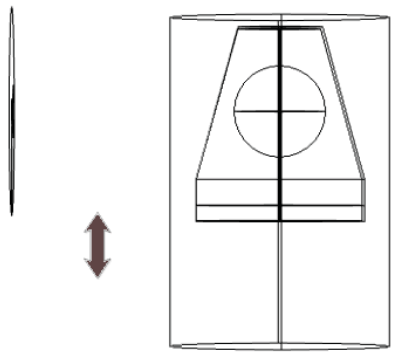

Fig. 4.33 Vertical displacement direction

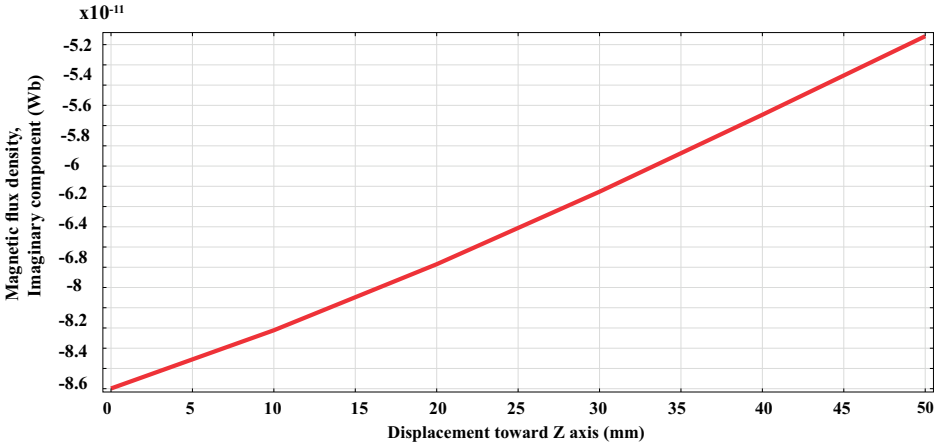

Fig. 4.34 System's sensitivity to displacement toward Z axis

Table 4.8 Magnetic flux density changes due to displacement toward Z axis

Object displacement toward Z axis (mm)	Magnetic flux density (Wb)
0	1.78 E-10 - 8.59 E-11 i
10	1.69 E-10 - 8.02 E-11 i
20	1.58 E-10 - 7.36 E-11 i
30	1.45 E-10 - 6.65 E-11 i
40	1.30 E-10 - 5.89 E-11 i
50	1.12 E-10 - 5.11 E-11 i

4.4.3 Displacement of the object toward sensors (Y axis)

In section 4.3, while simulating the breathing, we have considered a small movement toward the body and the results showed that the secondary signal is more affected by displacement rather than the conductivity. In this set of simulations, the distance between the body and the sensors changed from 65 mm to 35 mm. Table 4.9 shows the results. The real component increases up to 35% when the distance between the object (chest) and the sensors decrease from 65 to 35. On the other hand, the imaginary component grows rapidly getting closer to the

sensors. At 50 mm, the signal is almost 100% bigger than when the distance is 65 mm.

Table 4.9 Magnetic flux density changes due to displacement toward Y axis

Distance from the sensors (mm)	Magnetic flux density, y component (Wb)
65	1.37 E-10 - 5.23 E-11 i
60	1.51 E-10 - 6.16 E-11 i
55	1.65 E-10 - 7.27 E-11 i
50	1.78 E-10 - 8.59 E-11 i
45	1.90 E-10 - 1.01 E-10 i
40	2.02 E-10 - 1.20 E-10 i
35	2.14 E-10 - 1.43 E-10 i

4.5 Discussions and Conclusions

In this chapter, the development steps toward designing the magnetic induction based system for vital sign monitoring were described in detail.

It has been demonstrated that the adjacent coils structure of excitation and detection coils, is very sensitive to the displacements and also the impact of the capacitive coupling is higher in comparison to the asymmetric planar gradiometer (APG) structure we described and used later.

As described fully, the APG designed in a way to minimize the impact of the primary magnetic field on the small secondary signal detection (from the physiological activities).

The designed circuits for amplification and detection of the vital signs' contribution (secondary signal) are based on the simplicity and low-cost principles. The complete design was thoroughly studied for different parameters that can affect the received signal and alter it.

The new gradiometer based on concentric coils was designed using COMSOL to calculate and determine the diameters of the coils to fully cancel the primary field.

We have simulated the physiological and position changes to calculate the expected signals extracted from the new coaxial planar gradiometer. Coupling

mechanisms and capacitive coupling between coils and the object were analysed and circuit models were built using coupling coefficients and other parameters for full system simulation.
Based on the obtained results, the phase shift for the direct capacitive coupling would be around one degree. If the experimental results show higher shifts, it is due to the other impacts such as coupling to the ground.
Breathing's impact on the received signal was studied by analysing the impacts of a 3 mm change -which is equivalent to 0.5 litre of air change in the lungs- in the distance between chest and the sensors head, together with the passive electrical parameters (conductivity, permittivity) changes associated with breathing.
Spatial coverage of the system for a reliable detection was both simulated and measured experimentally. Assuming that the surface of the bed is on XY plane, the described system has a reliable coverage of about 8 cm for the displacements along $\pm$X. For the displacements along the Y axis, the coverage is higher but then the detected signal in different locations along Y axis could be a contribution of lungs, heart and also other abdominal body organs.

References

[1] Hadiseh Mahdavi and Javier Rosell-Ferrer. A magnetic induction measurement system for adult vital sign monitoring : evaluation of capacitive and inductive effects. In *XV Int. Conf. on Electrical Bio-Impedance & XIV Conf. on Electrical Impedance Tomography*, volume 012085, 2013. doi: 10.1088/1742-6596/434/1/012085.

[2] A Barai, S Watson, H Griffiths, and R Patz. Magnetic induction spectroscopy: non-contact measurement of the electrical conductivity spectra of biological samples. *Measurement Science and Technology*, 23(8):085501, aug 2012. ISSN 0957-0233.

[3] H Griffiths, W Gough, S Watson, and R J Williams. Residual capacitive coupling and the measurement of permittivity in magnetic induction tomography. *Physiological measurement*, 28(7):S301–11, jul 2007. ISSN 0967-3334. doi: 10.1088/0967-3334/28/7/S23.

[4] S Watson, C H Igney, O Dössel, R J Williams, and H Griffiths. A comparison of sensors for minimizing the primary signal in planar-array magnetic induction tomography. *Physiological measurement*, 26(2):S319–31, apr 2005. ISSN 0967-3334. doi: 10.1088/0967-3334/26/2/029. URL http://www.ncbi.nlm.nih.gov/pubmed/15798244.

[5] J Rosell, R Casañas, and H Scharfetter. Sensitivity maps and system requirements for magnetic induction tomography using a planar gradiometer. *Physiological Measurement*, 22(1):121–130, 2001. ISSN 09673334.

[6] Hermann Scharfetter, Stephan Rauchenzauner, Robert Merwa, O Biró, and Karl Hollaus. Planar gradiometer for magnetic induction tomography (MIT): theoretical and experimental sensitivity maps for a low-contrast phantom. *Physiological Measurement*, 25(1):325–333, feb 2004. ISSN 0967-3334. doi: 10.1088/0967-3334/25/1/036. URL http://stacks.iop.org/0967-3334/25/i=1/a=036?key=crossref.10b6a743b8f86af39d4109131ddf0bde.

[7] Javier Rosell-Ferrer, Claudia Hannelore Igney, and Matthias Hamsch. Planar coil arranement for a magnetic induction impedance measurement apparatus, 2012.

[8] Harold A. Wheeler. Simple inductance formulas for radio coils. *Proceedings of the Institute of Radio Engineers*, 16(10):1398–1400, 1928. ISSN 07315996. doi: 10.1109/JRPROC.1928.221309.

[9] Sunderarajan S. Mohan, Maria Del Mar Hershenson, Stephen P. Boyd, and Thomas H. Lee. Simple accurate expressions for planar spiral inductances. *IEEE Journal of Solid-State Circuits*, 34(10):1419–1420, 1999. ISSN 00189200. doi: 10.1109/4.792620.

[10] H Griffiths, W.R. Stewart, and W Gough. Magnetic Induction Tomography: A Measuring System for Biological Tissues. *Annals of the New York Academy of Sciences*, 1999.

[11] D Goss, RO Mackin, E Crescenzo, HS Tapp, and AJ Peyton. Understanding the coupling mechanisms in high frequency EMT. In *3rd World congress on industrial process tomography*, page 364/369, Banff, 2002.

[12] B Rigaud, P Morucci, and N Chauveau. Bioelectrical impedance techniques in medicine. *Critical Reviews in Biomedical Engineering*, 24, 1996.

Chapter 5

Experimental results

5.1 Introduction

The experimental setup for simulation verification and experiments with phantom consists of the coils, acquisition system and BIOPAC MP36. For experiments with volunteers pulse plethysmogram (PPG) sensor and pressure transducer of the BIOPAC-MP36 are used. The complete block diagram of the system is shown in figure 4.12 in chapter 4.

The coils are placed symmetrically with a 2 mm distance from each other. The distance between the coils and the object under test/the volunteer is either 5 cm or 20 cm which will be indicated in the description of each experiment. Unless stated, the vital sign monitoring experiments took 100 seconds and the sampling frequency was 500 sample per second.

No metallic parts or wire is used orthogonal to the field lines. The bed base and the mattress are all made with plastic, foam or wood in order to avoid any systematic error due to movement or presence of well-conducting and/or ferromagnetic material near the object space. Measurement protocol for the experiment is explained in the related section. The experimental setup for vital sign monitoring is illustrated in figure 5.1.

Fig. 5.1 Experimental setup

5.2 Linearity with conductivity changes

5.2.1 Experiment description

To evaluate the response of the system to different conductivities an experiment was performed using saline solution. Six different conductivities obtained by gradually adding Sodium Chloride to a 1-litre bottle of distilled water.
The separation between the sensor head and the bottle was 5 cm and the bottle was placed centrally regarding the sensors. Figure 5.2a and 5.2b shows the experimental setup and also the simulation model for this experiment.

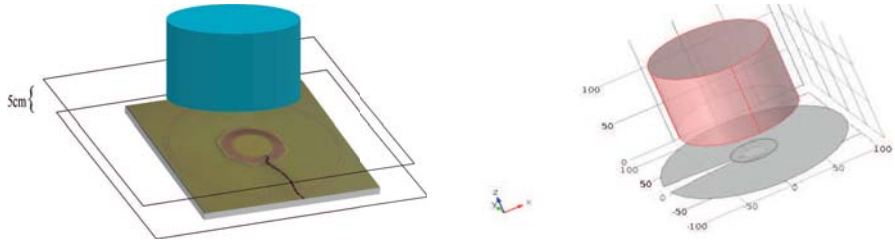

(a) Saline solution experiment setup (b) Saline solution simulation model in COMSOL

Fig. 5.2 Evaluation of system's sensitivity to conductivity changes, experimental set-up and simulation model

5.2.2 Results and discussions

The measured real and imaginary part of the received signals (due to changes in conductivity) are shown in figure 5.4. Figures 5.3 and 5.5 are the expected values from theoretical calculations based on the main equation of MI systems 5.1. These results are obtained after the phase shift calibration of the free space.

$$\Delta B = k\omega(-j\sigma + \omega\varepsilon) \tag{5.1}$$

The linearity of the received signal with changes in conductivity can be seen in the experimental results and it is in accordance with the simulation and theoretical estimations.
The practical maximum cancellation ratio obtained in experiments (adjustments of the coils) was measured as 150 times. To obtain the same real part in the experiments as in the theory/simulations a cancellation factor of 10^5 is necessary. On the other hand, the results for the real part of the signal (shown in 5.4) is not zero because:

- the cancellation of the primary field is not ideal so a part of this signal is due to the residual primary background signal
- the real part due to the permittivity of the tissues (equation 5.1) is orders of magnitude lower than the residual signal from the primary field
- the existence of the electric field coupling (explained in detail in 4)

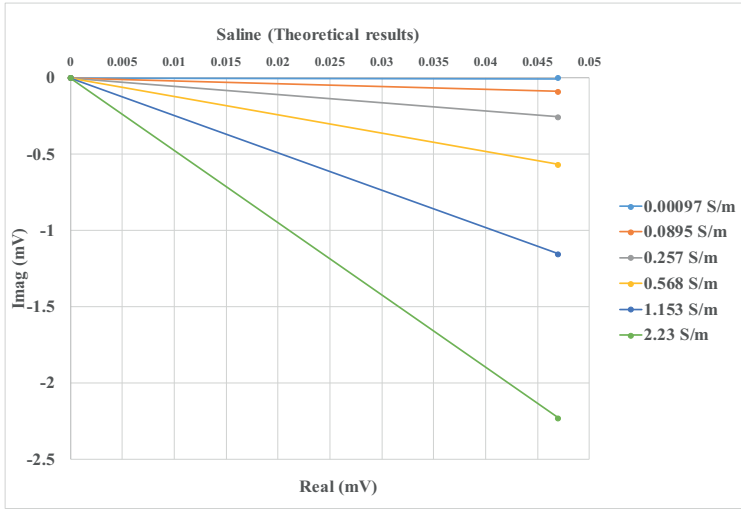

Fig. 5.3 Calculated real and imaginary components of the signal for different conductivities of saline solution

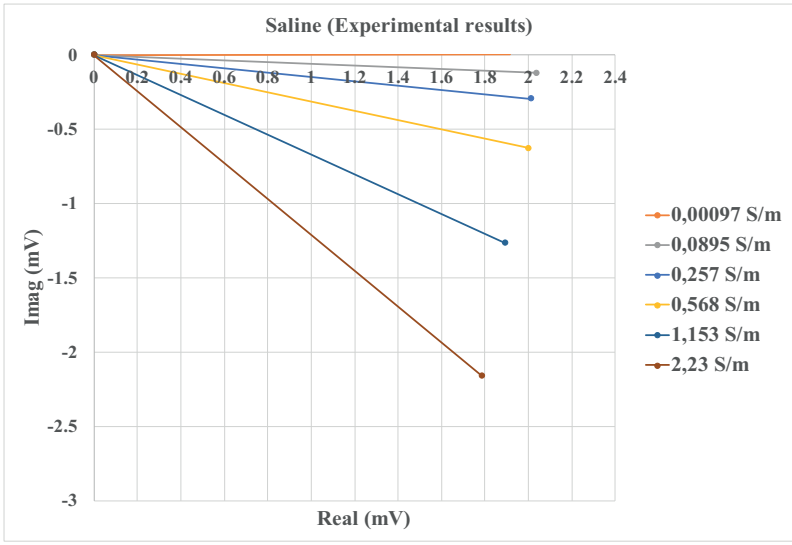

Fig. 5.4 Measured signal, real and imaginary components for different conductivities of saline solution

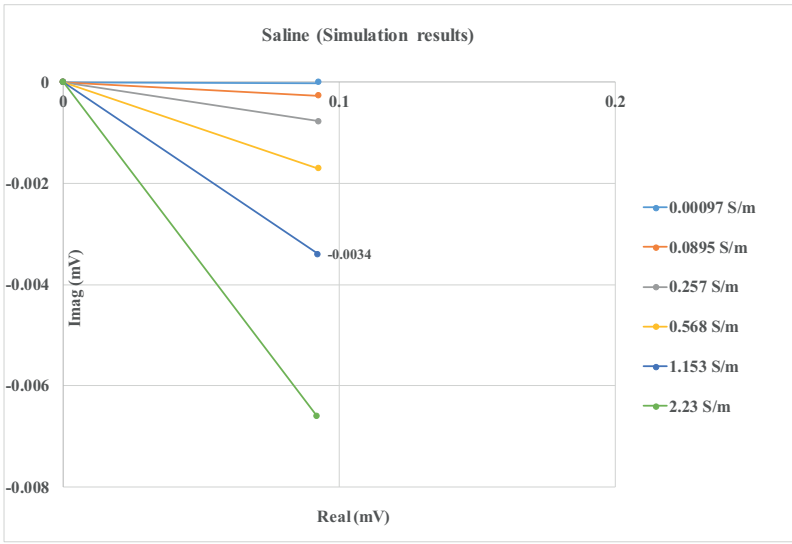

Fig. 5.5 Simulated real and imaginary components of the signal for different conductivities of saline solution

5.3 Sensitivity to displacement

5.3.1 Experiment description

Spatial coverage of the system for reliable detection was measured experimentally. The sensitivity of the system to the movements and displacements (which was simulated and studied in chapter 4) are examined with experiments. An 8-litre bottle of saline solution with a conductivity of $0.8 S/m$ was moved to the sides (X axis). The steps of displacement was 2 cm and the bottle moved up to 14 cm to each side. The distance between the sensor and the saline bottle was 10 cm.

5.3.2 Results and discussions

Figure 5.7 shows the real and imaginary component of the detected signal (after amplification). As the figure points out, at 8 cm of movement from the center of the coils' plane, the imaginary component of the signal -which is the contribution of our saline solution bottle- decrease about 46%, very close to the simulation results (see table 4.7). Assuming that the surface of the bed is on XY plane, this confirms a margin of about 8-10 cm sensitive region on each side of the coil center ($\pm X$). For the displacements along the Y axis, the coverage is higher but then the detected signal in different locations along Y axis could be a contribution of lungs, heart and also other abdominal body organs.

Fig. 5.6 Saline bottle over sensor for displacement experiment

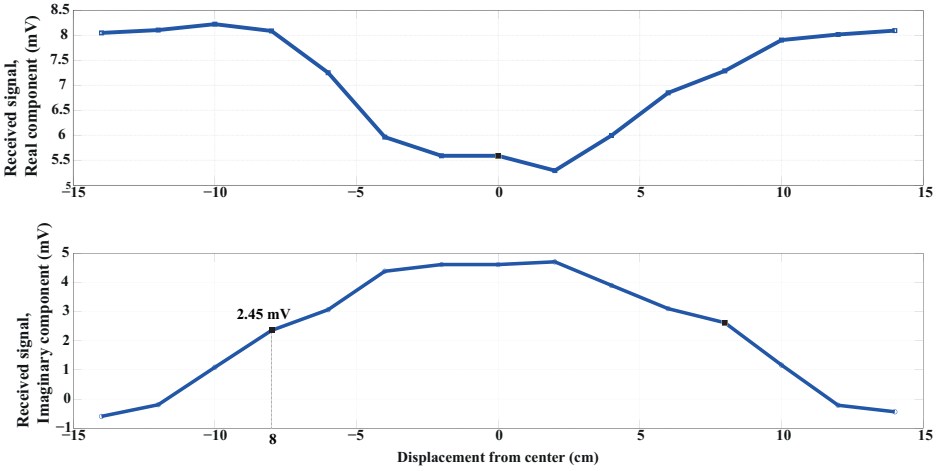

Fig. 5.7 Sensitivity experiments, received signal's component

5.4 Vital sign monitoring

5.4.1 Experiment description

In these experiments, the distance between the sensor head and the volunteer was either 5 cm or 20 cm (5 cm between sensor and mattress and 15 cm width of the mattress). The 5 cm distance was obtained by placing the excitation and APG (sensors) inside the mattress. There is no direct contact between the patient (volunteer)'s body with the sensors. The experiments start with breathing normally, follows by a period of apnea and back again to normal breathing. The experiments took 100 seconds and in order to avoid motion artifacts and the volunteers were asked to stay still. Body posture in these experiments was prone and supine positions and additional experiments on sides position.

Fig. 5.8 Sensors' position, 20 cm distance between body and sensor head

As it could be seen in figure 5.8, the pressure sensor is placed directly under the mattress. The PPG sensor is connected to the patients finger to record the pulses through Photoplethysmography.

5.4.2 Noise of the system

Figure 5.9 shows the normalized signals received when there is no object over the bed (noise) and the signal received from a volunteer in the prone position. The distance between the volunteer and the sensor head is 5 cm. As it can be seen, the noise level is much lower than the breathing signal level. The phase changes due to cardiac activity during apnea period is around 30 millidegree while the noise level is around 15 millidegree.

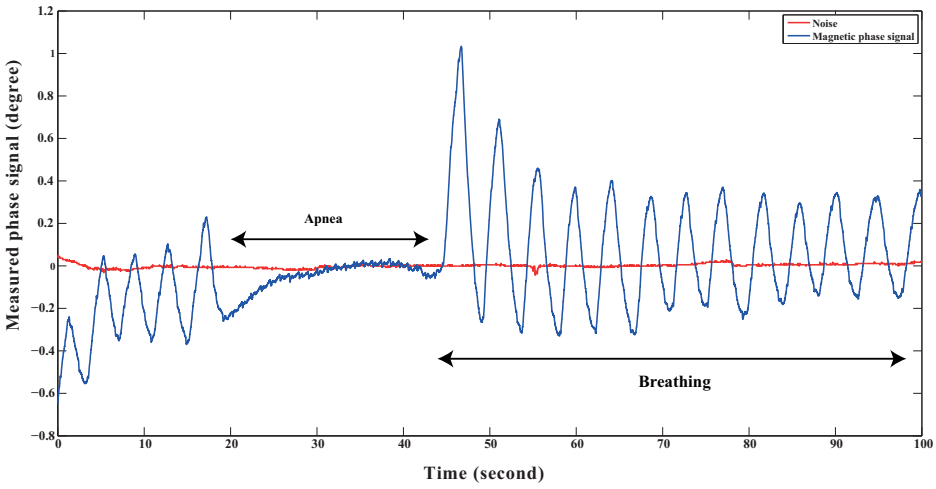

Fig. 5.9 Magnetic phase signal, free space signal (noise) versus volunteers measured signal

5.4.3 20 cm separation

Figure 5.10 shows the signals obtained from the person over the bed with a 20 cm distance from the sensors at supine position.

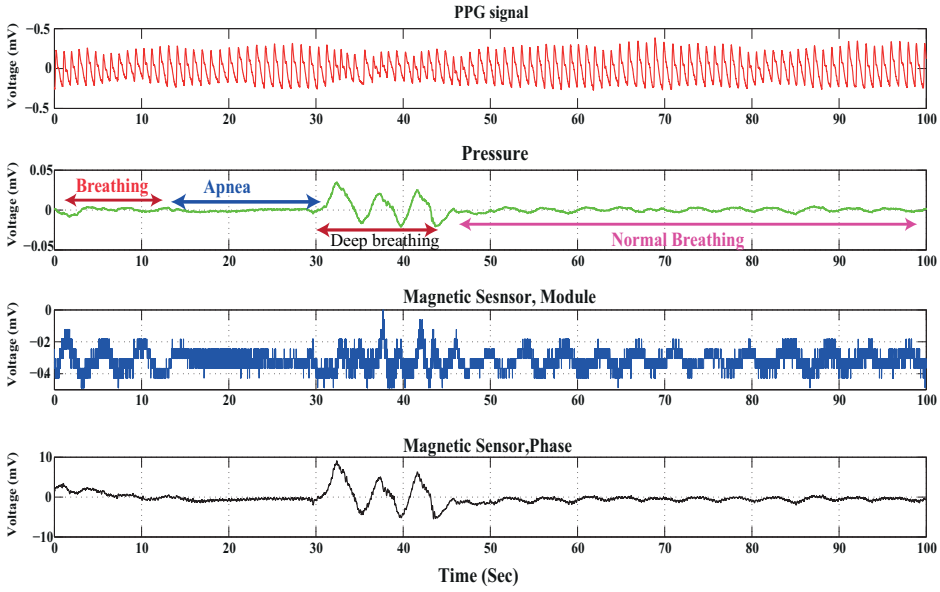

Fig. 5.10 Vital sign monitoring, supine position (20 cm separation)

The signals received at 20 cm were very poor and at the levels of quantification noise especially for the magnitude. This lead us to reduce the distance and use the 5 cm distance as a more appropriate distance for measuring the signals.

5.4.4 5 cm separation

Figures below show the 100 seconds of vital sign registering in prone and supine position. The received signal while the volunteer stop breathing (apnea region) is zoomed and compared with the reference signal. Figure 5.11 and 5.12 show the raw signal without filtering. The figures with a zoom in apnea region are filtered signal. The filter is an order 4 Butterworth filter with a cut-off frequency of 0.4 Hz and the applied digital filter from BIOPAC is a high pass filter with cut off frequency of 0.05 Hz.

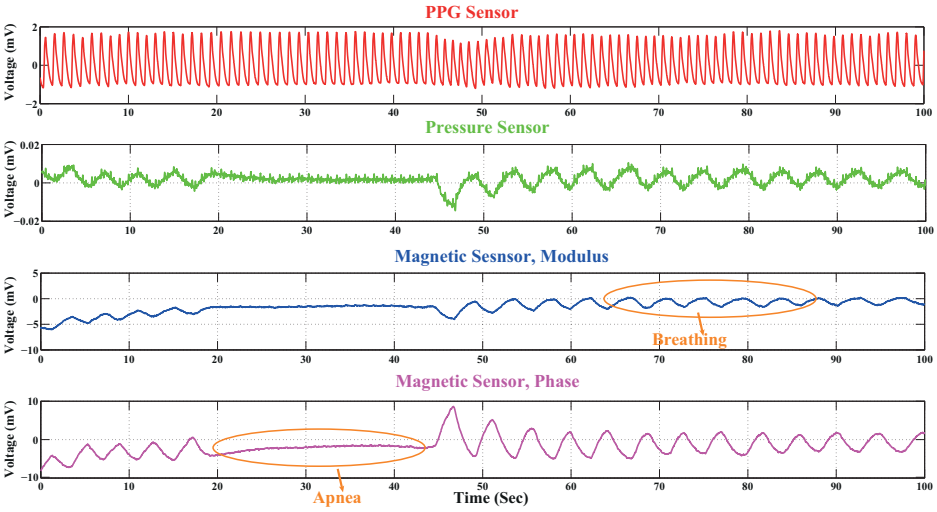

Fig. 5.11 Vital sign monitoring, supine position (5 cm separation)

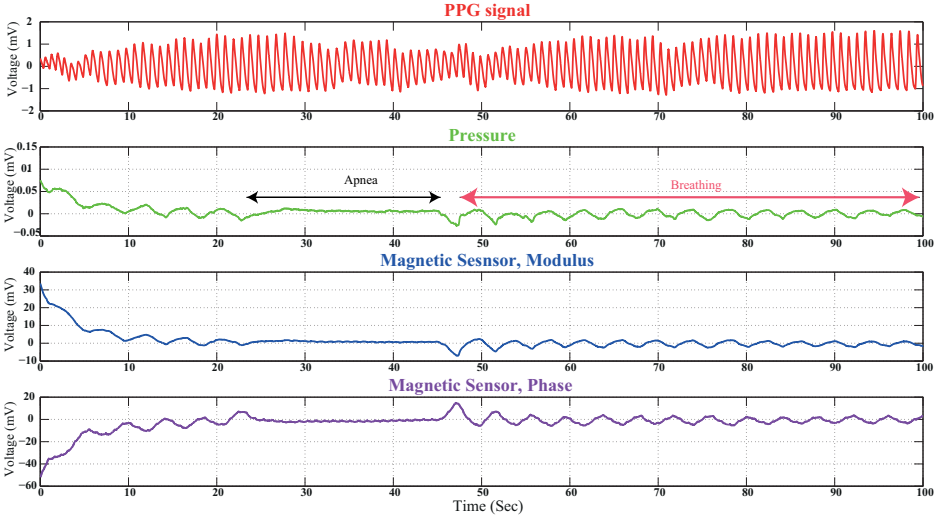

Fig. 5.12 Vital sign monitoring, prone position (5 cm separation)

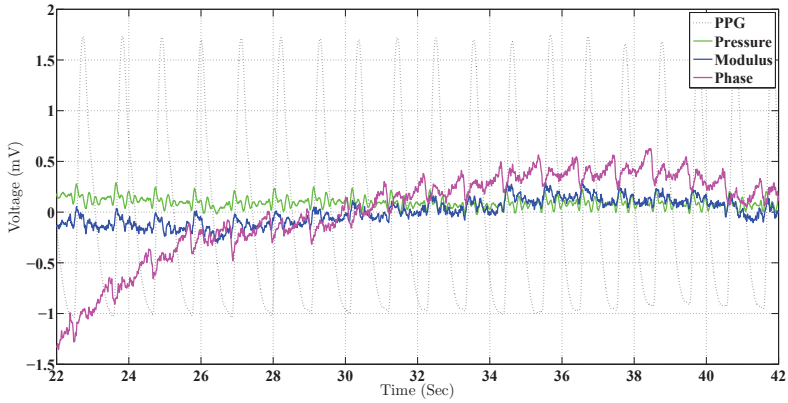

Fig. 5.13 Apnea signal in **Supine** position, Note that the signal from pressure sensor has been scaled 50 times for demonstration reasons

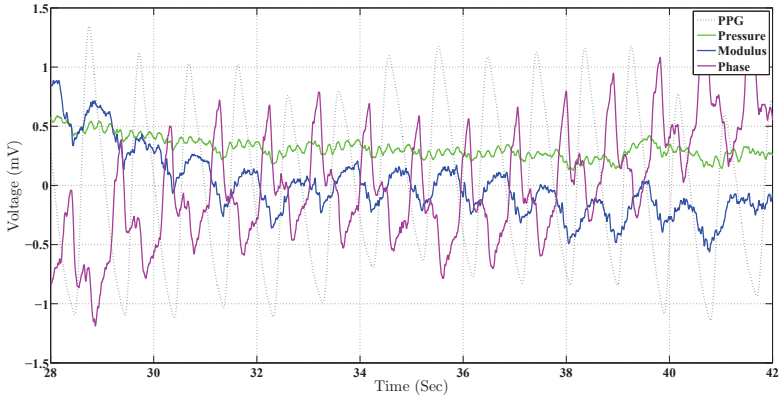

Fig. 5.14 Apnea signal in **Prone** position, Note that the signal from pressure sensor has been scaled 50 times for demonstration reasons

Figures 5.13 and 5.14 provide a comparison insight of the cardiac activity at the apnea period of prone and supine position, for all four sensors. The pressure signal has been enlarged for demonstration since the received signal from this sensor is very small. As it could be seen, monitoring breathing signal is not an issue and both MI and pressure sensors can detect it.

In MI simulations (with a 5 cm distance between the body and the coils), chang-

ing the conductivity and volume of the lungs from deflated to inflated mode, cause a 6.8 percent decrease in the imaginary component of the signal while the real component grows about 0.19 percent.
However, inhalation of air into the lungs produce a small increase in the thorax volume which could be considered as a small movement toward the sensors. An increase of 0.5 litre in thorax's volume, results in an approximate 3 mm displacement of the body toward the coils. This modification in distance affects both components of the received signal. The imaginary component, in this case, decreases 0.21 percent changing from deflation to inflation mode while the increase in the real part of the signal is 4.3 percent.
The experiments results' are in accordance with the results from simulations. As shown in the figures, when the lungs are filled with air (inflation mode) the modulus of the magnetic signal increases while the phase decreases. The decrease in phase signal is due to decrement of conductivity of the lungs while the increment in the modulus could be caused by the chest's expansion which slightly changes the distance between the sensors and the body, and also modify the distribution of the currents in the surface.
A change in the surface geometry of the object or the patient, close to the coils, will introduce a change in the capacitive coupling and also in the received secondary magnetic field. Both cases will produce a change relative to the posture of the patient or body movements related to breathing or cardiac activity. The advantage of the magnetic system is that if there is no movement, the magnetic field that penetrates the body still produces a secondary signal that could be detected.

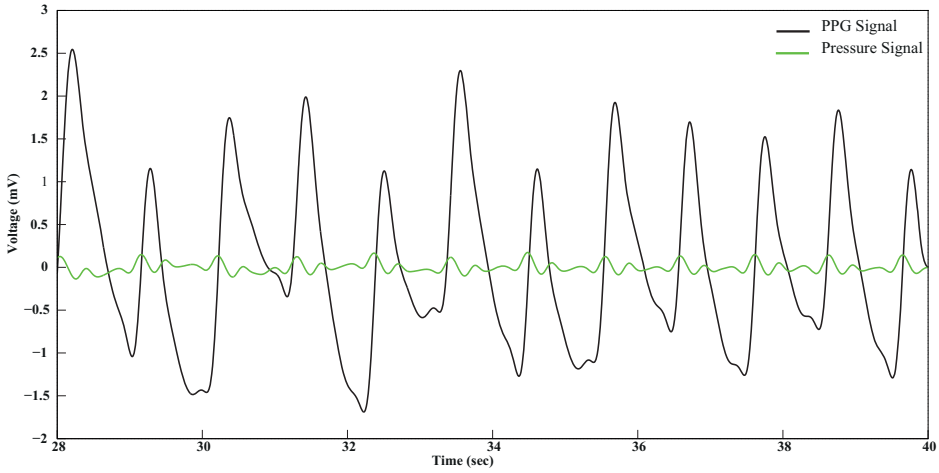

Fig. 5.15 Supine apnea, PPG and pressure sensor signal (5 cm separation)

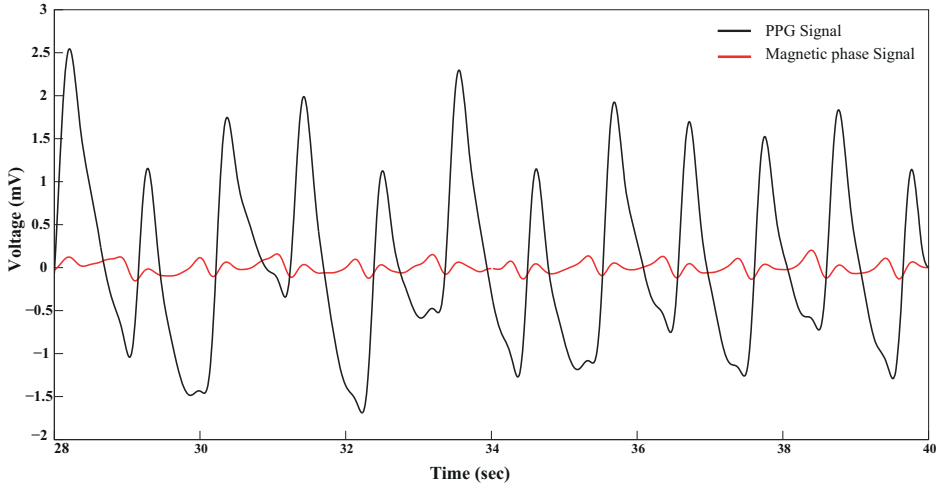

Fig. 5.16 Supine apnea, PPG and magnetic phase signal (5 cm separation)

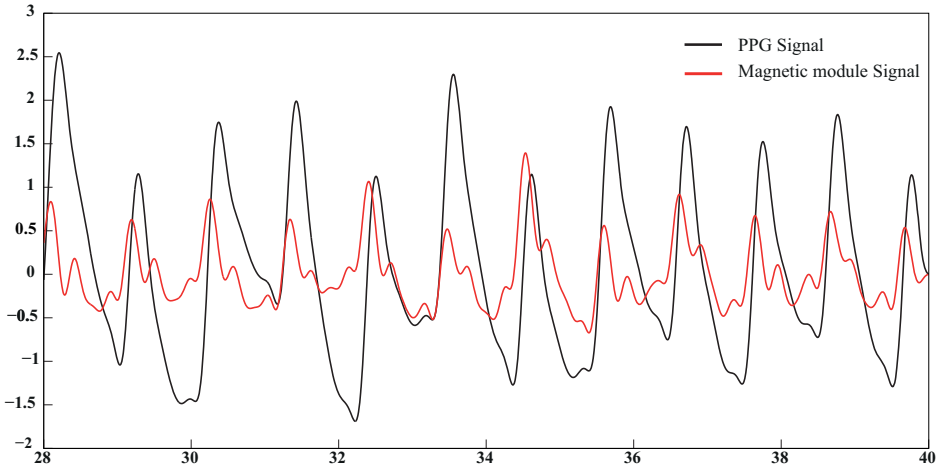

Fig. 5.17 Supine apnea, PPG and magnetic modulus signal (5 cm separation)

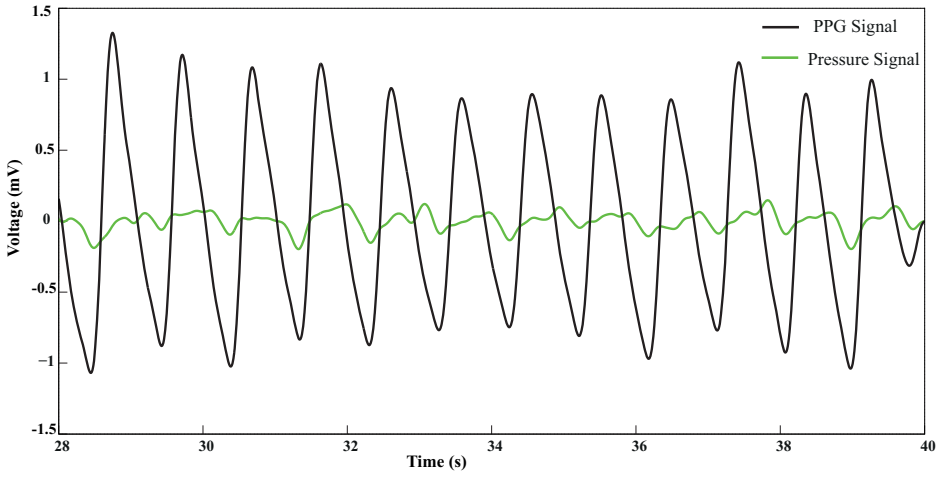

Fig. 5.18 Prone apnea, PPG and pressure sensor signal (5 cm separation)

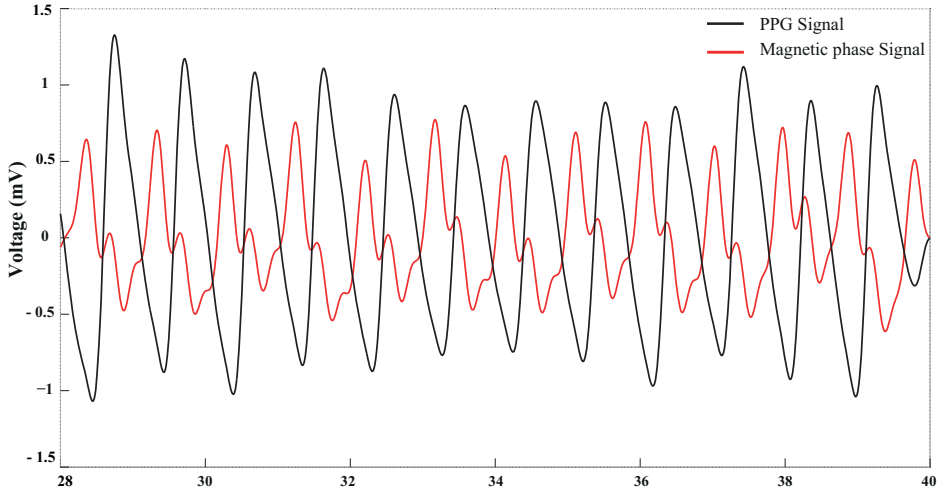

Fig. 5.19 Prone apnea, PPG and magnetic phase signal (5 cm separation)

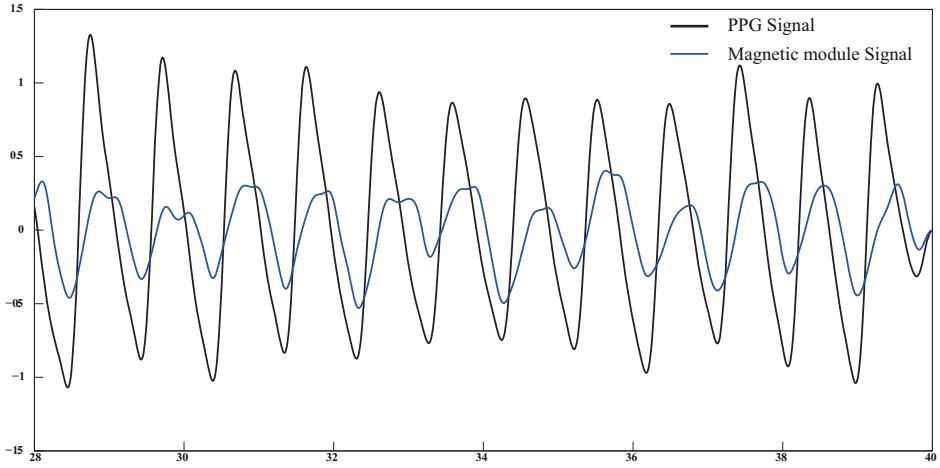

Fig. 5.20 Prone apnea, PPG and magnetic modulus signal (5 cm separation)

Comparing the signals of supine and prone positions indicates that the signal from prone position contains more information in regards to cardiac activity due to its position advantage. In the prone position, the sensors are closer to the heart, to the blood volume changes in heart's major vessels (Aorta) and to the lung perfusion while in the supine position, the distance is higher and other struc-

tures like vertebral column are located in between. However, both supine and prone positions show more reliable signals than the pressure sensor's outcomes. The signal was processed and studied both in time and frequency domain. For studying the signals in the frequency domain and check the coherency of the signals with the cardiac activity's frequency we used Welch method to analyze the apnea signal and study the power spectral density.

The Welch's method for the calculation of PSD (power spectral density) is a non-parametric method that has some advantages as the simplicity of the algorithm employed (Fast Fourier Transform) and the high processing speed. This method allows the calculation of periodograms of short segments of the signal (in our case, length of the signal divided by four) and their average with the aim of reducing the estimator variance (leakage).

Additionally, it is possible the application of different types of windows (rectangular, triangular, Hanning or Hamming) in each segment of the signal in order to optimize the commitment between the estimator variance and the resolution. We have applied a rectangular window with 50% overlapping between segments.

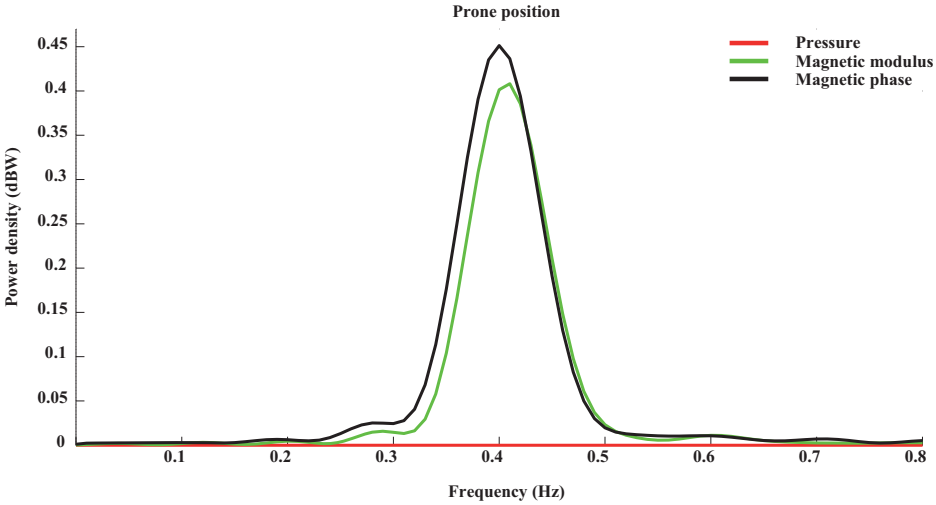

Fig. 5.21 Frequency spectrum of the received signal for breathing, prone position (5 cm separation, normalized to noise level)

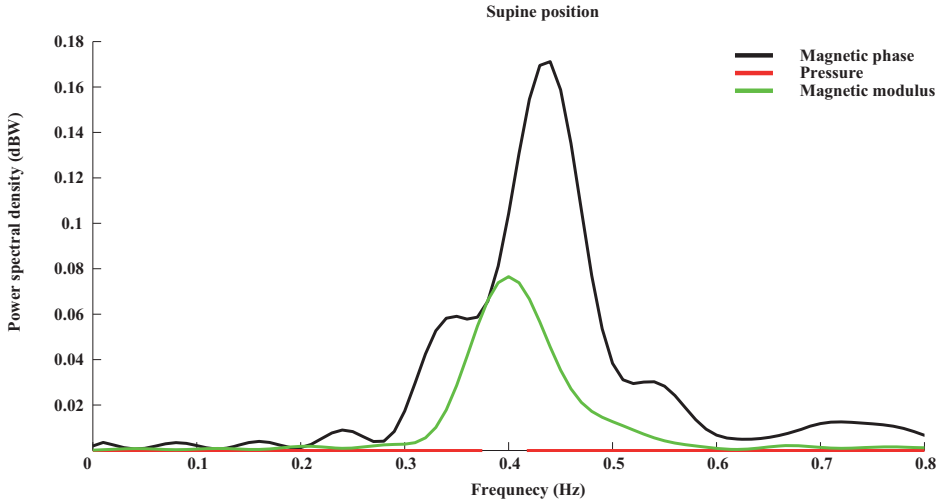

Fig. 5.22 Frequency spectrum of the received signal for breathing, supine position (5 cm separation, normalized to noise level)

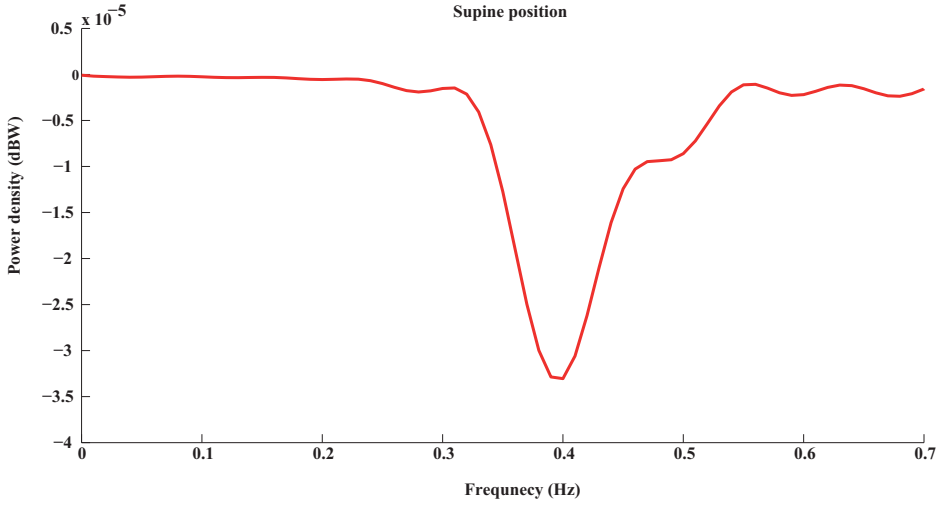

Fig. 5.23 Frequency spectrum of the received signal for breathing from pressure sensor, prone position (5 cm separation, normalized to noise level)

Figures 5.21 and 5.22 show the power spectrum for the breathing frequency received from magnetic and pressure sensors normalized to the noise level, in

prone and supine positions respectively. All three signals from both magnetic and pressure sensors show a component at 0.4 Hz. The Magnetic modulus and the pressure signals are at the noise level while the magnetic phase signal is less noisy in particular in the prone position. Figures 5.23 shows a focused image of the pressure signal in the supine position.
At frequencies around 1 Hz, the cardiac activity frequency can be seen in Magnetic phase and modulus but hardly in the pressure sensor. The signal from the pressure sensor at 1 Hz is a very low power signal faded in noise. Figure 5.24 shows the spectrum at 1 Hz for prone position.

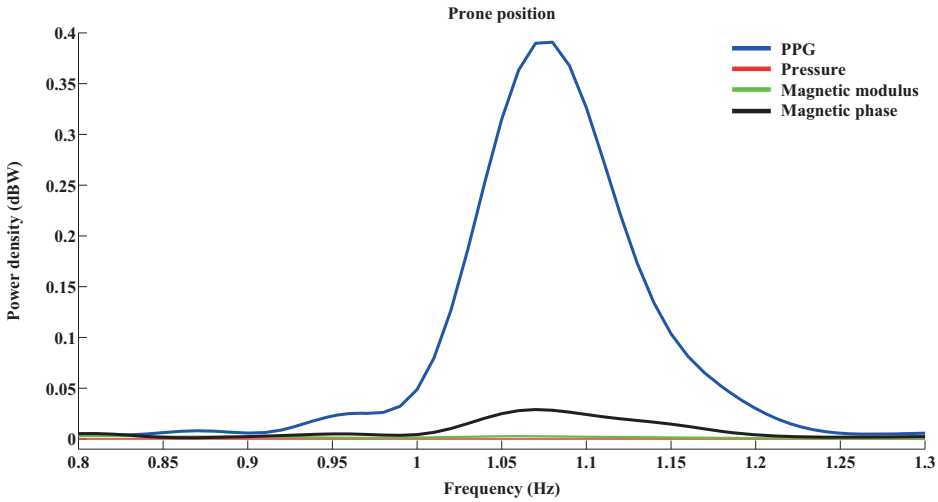

Fig. 5.24 Frequency spectrum of the received signal for cardiac activity, prone position (5 cm separation, normalized to noise level)

Looking at the unfiltered signal received by magnetic sensor (figure 5.25), comparing the apnea signal of magnetic phase signal and the PPG, it can be seen that the signal contains more information than the PPG signal. This information could be related to other phases of the cardiac cycle, sourcing from conductivity changes or mechanical changes inside the heart cavity or chest.

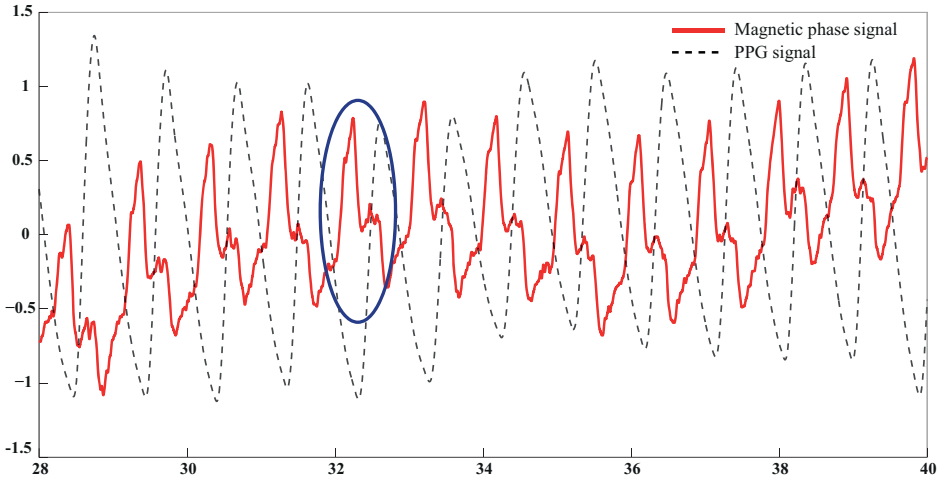

Fig. 5.25 PPG and magnetic phase unfiltered signals in apnea phase, prone position (5 cm separation)

Detection of the breathing signal is not an issue for the system, further experiments with male volunteers showed that the people's breathing habits affect the received signal. The difficulty rises especially when measuring people who do diaphragmatic breathing [1]. Breathing through stomach causes bigger periodic body movements which could affect the received signal. It could modify the distance between the sensor and the body or change the current distributions. In our experiments, the measurements with people who were chest breathing were in accordance with the reference signals [**?**].

[1] stomach breathing

5.4.5 Lateral position

Lateral recumbent positions are other two positions which were measured for five volunteers in addition to the supine and prone positions. Focusing on the received signal by the magnetic sensor, figure 5.26 show the received signal of four positions of a single volunteer (our best case); prone, supine, right and left sides at a 20 cm distance. It could be said that the left size position due to it's position advantage of being closer to the heart shows better signals of heart activity from the right side position.

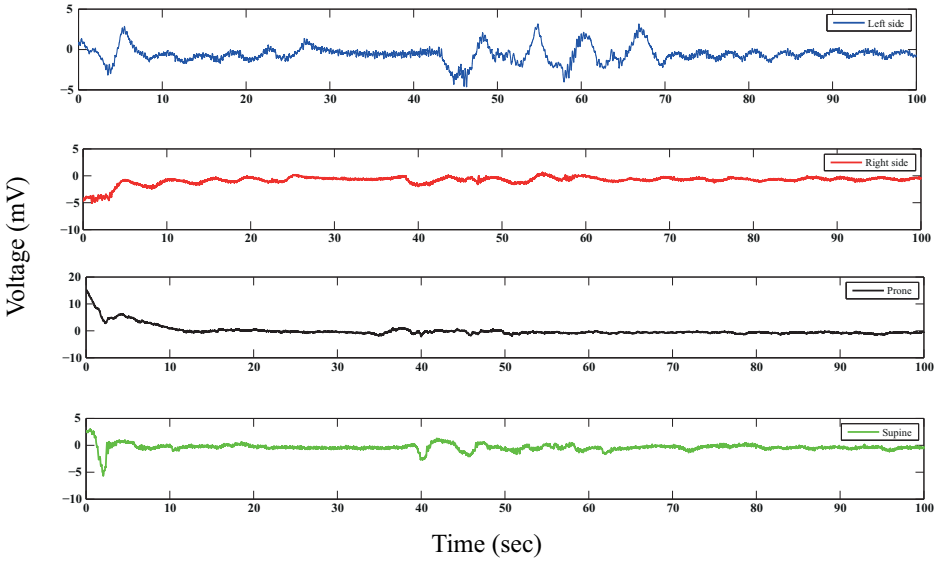

Fig. 5.26 Magnetic phase signal of a volunteer in 4 different positions

The quality of the signal was not good at 20 cm due to high level interference.

Chapter 6

Conclusions and future works

6.1 Conclusions

A new magnetic induction sensor system was developed and described in this thesis. As explained in detail, the system is a non-contact planar system designed to be placed under the bed or mattress for unobtrusive monitoring applications such as sleep monitoring, neonates monitoring, etc.
The system consists of one coil for excitation, one for detection and an electronic box for amplification and demodulation of the received signal.
The whole system is designed having a cheap, straightforward design mindset. The aim was to avoid complexities and provide a design which could be easily installed and used without the need of an expert technician.
The system works based on exposure of the electromagnetic fields for a continuous time so it has been studied (by simulation) against safety standards to ensure the safety of the system for being used at the controlled or/and uncontrolled environments corresponding to occupational and general public exposures.
The results show that the system placed at 5 cm of the patient's chest, can detect the presence of the patient on the bed, breathing and also cardiac activity. The signal levels decrease with the increment of the distance. Based on the models, the sensitivity to chest movements (due to physiological activities) is higher than

the sensitivity to the conductivity changes.
The new gradiometer based on concentric coils was designed using COMSOL to calculate and determine the diameters of the coils to fully cancel the primary field. The experiments with the new gradiometers confirmed the estimated results from the simulations.
The physiological and position changes to calculate the expected signals extracted from the new coaxial planar gradiometer were modeled and simulated. Coupling mechanisms and capacitive coupling between coils and the object were analysed and circuit models were built using coupling coefficients and other parameters for full system simulation.
Based on the obtained results, the phase shift for the direct capacitive coupling would be around one degree. The experimental results showed higher shifts, which is due to the other impacts such as coupling to the ground.
Breathing's impact on the received signal were studied by analysing the impacts of a 3 mm change -which is equivalent to 0.5 litre of air change in the lungs- in the distance between chest and the sensors head, together with the passive electrical parameters (conductivity, permittivity) changes associated with breathing.
Both pressure and magnetic sensors can detect breathing signal. However, the detected signal by the pressure sensor, has a much lower amplitude in comparison with magnetic signal and depends on the position of the body may fade (based on the experiments). Cardiac activity is also detected by the magnetic system which in majority of the measurement cases, the magnetic phase signal showed better results than the magnetic modulus sensor as expected by the theory.
The magnetic phase signal is more sensitive than the modulus signal and is also more robust regarding the motion artifacts and interferences. In addition, the magnetic phase signal contains more information of the heart activity that need further studies to identify the sources.
There are various parameters that affect the signal received by the sensors. Displacement of the thorax or abdomen (external shape changes) and Internal eddy currents (changes on internal conductivities) modify the received signal at the APG. But the sources of these parameters could not be identified easily. Thorax or abdomen displacements can produce changes in surface eddy currents and/or in the capacitive couplings and modify the signal. On the other hand, the internal eddy currents and changes in conductivity could be due to lung perfusion,

muscle perfusion or blood volume changes in the heart or aorta.
There is a difference between the signal detected in supine and prone position which could be because of the proximity of patient's heart position to the sensors in prone position. Comparing signals from MI phase and modulus points out that in some cases/positions the cardiac signal is better detected in either of signals From the experiments with volunteers, it could be concluded that the breathing habits (chest breathing or belly breathing) of people affects the signal received at the sensors. The less the distance between sensors head and the body/object, the more information will be received at the detector.
A 5 cm distance proved to be an acceptable value for the separation. The sensitive area of the bed is directly related to the sensors' radius and the body size. In our design a radius of 8 to 10 cm secure the desired sensitivity to detect vital signs. In lateral recumbent positions the variability of the signals were high and it is difficult to make a definitive conclusion but our experiment showed that the left side position (lying over the left shoulder) shows higher sensitivity to cardiac activity while for breathing, no big difference has been identified.

6.2 Future works

The system could be improved and completed from the electronic point of view. Embedding a function generator chip, using bluetooth for communication aims, improving the sensitivity and rigidness of the system to motions and displacements are among the possible system improvements. In addition, an analog coherent phase detector based on multipliers can be used to reduce the noise due to interferences.
However a more in-depth study is needed to identify the sources of the received signal by the magnetic sensor and the contribution of each of the assumed parameters.
The system and its design could be used in applications like smart mattresses, smart homes and neonates monitoring. The coils design and configuration could be applied to applications like smart textiles and wearables.